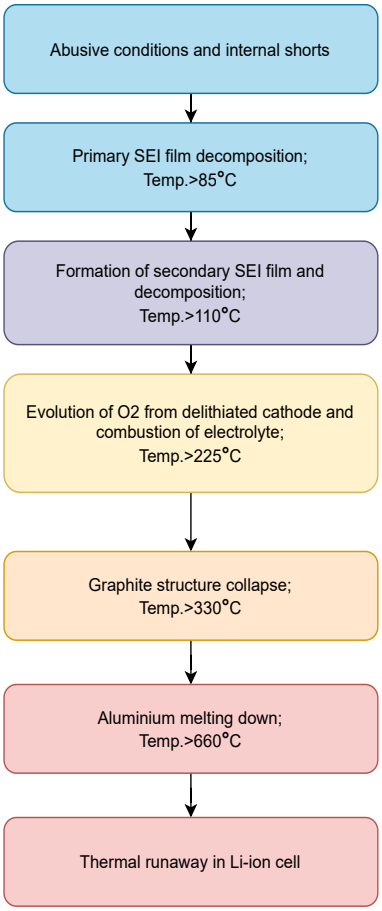

Lithium-ion Battery Fault Detection and Application on Reconfigurable Battery Systems

Master's thesis in Electric Power Engineering

Rahul Puthukode Ramakrishnan
Rohit Puthukode Ramakrishnan

Department of Electrical Engineering
CHALMERS UNIVERSITY OF TECHNOLOGY
Gothenburg, Sweden 2021
www.chalmers.se

Master's thesis 2021

Lithium-ion Battery Fault Detection and Application on Reconfigurable Battery Systems

Rahul Puthukode Ramakrishnan
Rohit Puthukode Ramakrishnan

CHALMERS
UNIVERSITY OF TECHNOLOGY

Department of Electrical Engineering
Electric Power Engineering
Chalmers University of Technology
Gothenburg, Sweden 2021

Lithium-ion Battery Fault Detection and Application on Reconfigurable Battery Systems

Examiner: Yujing Liu, Chalmers University of Technology

Supervisors: Emil Edvardsson, Knightec AB
Bowen Jiang, Chalmers University of Technology

Master's Thesis 2021
Electric Power Engineering
Department of Electrical Engineering
Chalmers University of Technology
SE-412 96 Gothenburg
Telephone +46 31 772 1000

Cover: Flowchart showing how thermal runaway develops in Li-ion cells.

Typeset in LaTeX
Printed by Chalmers Reproservice
Gothenburg, Sweden 2021

Lithium-ion battery fault detection and application on reconfigurable battery systems

Rahul Puthukode Ramakrishnan
Rohit Puthukode Ramakrishnan
Department of Electrical Engineering
Chalmers University of Technology

Abstract

In a traditional multi-cell Lithium-ion battery system, there could be issues that can be hazardous, posing safety threats to users due to different faults. The faults include over-discharge, over-charge, and internal short-circuit. These faults can damage the materials of the cells and lead to decreased lifespans and thermal instability. The internal short-circuit is one of the most dangerous faults. Most of the above-mentioned faults eventually lead to thermal runaway where high temperature and pressure will make the electrode reaction rate faster, increasing the battery temperature, leading to possible explosion and release of toxic gases.

Hence, it is important to detect these faults to decrease the safety risks that may result in the event of such adverse circumstances. This thesis aims to analyze the failure modes of the Lithium-ion cell and the reasons causing these failures. Modelling methods of these failures, particularly internal short-circuit, have been implemented and their impacts have been studied using Simulink and COMSOL Multiphysics. The applications of fault detection for various scenarios of internal short-circuit and different load conditions have also been studied. Respective results have been analyzed and a technological solution in the form of reconfigurable battery systems has been investigated as a means to mitigate these faults.

Keywords: Lithium-ion batteries, fault detection, battery internal short circuit, reconfigurable batteries, electric vehicles.

Acknowledgements

This thesis is a product of the unconditional support we received from our examiner Prof. Yujing Liu. We would like to express our sincere gratitude to him for having given us the opportunity to perform this thesis under his guidance.

We would also like to extend our heartfelt thanks to our academic supervisor Bowen Jiang without whose support this thesis would not be possible. His feedback during crucial junctures were invaluable to us in taking the thesis forward.

We would also like to express our profound appreciation to Emil Edvardssson from Knightec AB whose encouragement and advice during weekly meetings helped us immensely.

We would also like recognize the constant support and motivation received from our family without whom our dream of pursuing a master's degree from Chalmers University would not have been possible.

Rohit Puthukode Ramakrishnan & Rahul Puthukode Ramakrishnan
Gothenburg, October 2021

Contents

List of Figures

List of Tables

1

Introduction

The present-day environmental situation calls for use of sustainable forms of transport, among which Electric and Hybrid Vehicles are the most promising solutions. Owing to this, there is an enhanced need for safer battery systems to be used in Electric vehicles (EVs). This is keeping in mind that the battery is one of the most important and expensive components in the drivetrain of an EV. Li-ion batteries have improved in many features, particularly energy density, power density, and cycle life. However, battery safety still remains an area of focus for battery manufacturers, automotive OEMs, companies providing energy storage solutions and consumers.

In a traditional multi-cell battery system, there are issues which could be hazardous and pose safety threats due to different faults. The faults can be internal such as overcharge, over-discharge, thermal runaway, overheating, accelerated degradation, internal and external short circuit of the battery cells. Safety issues can also arise due to external faults like sensor (temperature, voltage and current) faults.

Faults like overcharge and overdischarge can damage the materials of the battery and lead to decreased lifespan and thermal instability. Internal short circuit and external short circuit can lead to thermal runaway. Accelerated degradation occurs due to fast-charging/discharging, over-charging/discharging, and low-temperature. Most of these faults eventually lead to thermal runaway where the high temperature and pressure will make the electrode reaction rate faster making the battery temperature even higher leading to possible explosion and release of toxic gases. Hence, it is important to detect these faults to decrease the safety risks and hazardous conditions that might result in the event of such faults.

A conventional multi-cell lithium ion battery pack has some disadvantages like capacity fading, cell voltage unbalance, and low reliability. To mitigate these issues, a reconfigurable battery system can be used. The advantages of reconfigurable battery systems are that the module-level topology can be dynamically reconfigured using active power electronic switches. Cell-level reconfigurability can also be based on conditions like the state of charge (SoC) and the state of health (SoH) of the cells. The other pros with a reconfigurable battery system are that it is capable of giving variable output voltages, providing possibilities of charge and thermal balancing with enhanced fault tolerance in addition to powering different vehicle equipment. Reconfigurable battery systems (RBS) are able to quickly disconnect the faulty cells providing fault isolation without the normal operation being affected. RBS is also

beneficial since additional balancing circuitry is not required. This is because the charge and temperature can be balanced by reconfiguration of cells leading to lower maintenance costs.

1.1 Thesis purpose

This thesis aims to analyze the failure modes of the Lithium-ion cell and the reasons causing the failures. Modelling methods of internal short-circuits will be discussed and implemented. Their impacts will be studied using appropriate simulations softwares. The applications of fault detection for various scenarios of internal short-circuit and different load conditions will be examined. Respective results will be reviewed and a solution mitigate these faults will be proposed.

1.2 Thesis scope

- The algorithms developed are suitable for Li-ion cell chemistry.
- The cell along with module level fault detection have been studied.
- Problems arising due to temperature variations have not been considered as part of this thesis.

1.3 Chapters

The report is assembled into different chapters.
Chapter 1-Theory: Contains the theoretical details of the thesis which would be used for analyzing the corresponding work.
Chapter 2-Methods: Discusses the methods followed in the thesis to implement the fault detection algorithms after cosimulation.
Chapter 3-Results: Presents results after simulation and implementation of battery fault detection algorithms.
Chapter 4-Conclusions & Future work: Contains the insights obtained from this thesis and recommendations for future work.

2
Background

This section gives an overview of the theoretical aspects needed to understand this thesis report.

2.1 Cell

The Lithium-ion or Li-ion cell is one of the most common types of cells used in electric vehicles. It is essentially an energy storage device (ESD), which is rechargeable, also called secondary type of batteries. A group of cells forms a Li-ion battery pack and the basic components of a Li-ion cell are the anode and cathode electrodes, a separator, electrolyte, current collectors and outer protective shell or case.

The cathode materials widely used in Li-ion cells are Lithium Nickel Manganese Cobalt Oxide (NMC), Lithium Manganese Oxide (LMO), Lithium Cobalt Oxide (LCO), Lithium Iron Phosphate (LFP) and Lithium Nickel Cobalt Aluminium Oxide (NCA). The most common cathode material used in EVs nowadays is the NMC type due to its high energy density and low self-discharge. The active materials are a combination of one of the above Lithium metal oxides along with a polymer binder and a conductive filler. They must be chemically stable and capable of diffusing the Li-ions with the ability to insert and remove the Li-ions without any structural changes.

The anode of the battery is usually made from a carbon-based material like Graphite or Graphene. These materials are abundant and are electrically conducting and can 'intercalate' the Li-ions to store charges. Silicon is also coming up as a possible alternate to carbon based anodes.

The electrolyte acts as a transport medium for the Lithium ions but not for the electrons. The liquid electrolytes are usually made of lithium salt like Lithium hexafluorophosphate ($LiPF_6$) dissolved in a mixture of organic solvents like carbonates.

The separator is an electrically insulating material placed between the anode and cathode. The separator helps prevent short circuit between the terminals and its micro-porous structure makes the movement of lithium ions possible.The current collectors of the battery system are placed at the electrodes to form a complete circuit and as a medium to transport electrons in the external circuit. Usually, Aluminium is used as the positive or cathodic current collector and Copper is used

as the negative or anodic current collector. The process of the Solid Electrolyte Interface (SEI) layer formation during the first charging event saves the electrolyte from degradation and prevents contact between the electrons and the electrolyte. In Li-ion cells, the electrolyte solvent molecules cover the Li-ions during charging which forms the SEI layer on reaction with Graphite at the electrode-electrolyte interface. A small percentage of Li-ions is consumed in the SEI layer formation and the growth of SEI layer can also lead to loss of usable Li-ions and over time result in capacity loss.

The reactions happening in a Li-ion battery during discharge process involves release of Lithium ions and electrons or oxidation at the negative electrode, and the reverse mechanism (reduction) at the positive electrode. Positively charged Li-ions arrive at the cathode using the electrolyte as a medium from the anode. The work in the circuit or the load is done by the electrons which traverse through cables and wires into the cathode from the anode as shown in Fig.2.1 [32]. This guided flow of electrons causes an electric current in the circuit. The smallest element in a battery is the cell which are connected to form modules and many such modules connected together form a battery pack. The series connection of the cells can increase the total voltage and the parallel connection of cells leads to the increase of the total capacity (Ah). The battery pack cells can be made of different cell types, namely cylindrical, prismatic of pouch types. Cylindrical type is the most widely used cell format and is easy to manufacture. Prismatic type has good space utilization but is expensive to manufacture. Pouch type has a simple and cost effective design but swelling of the cells is a problem.

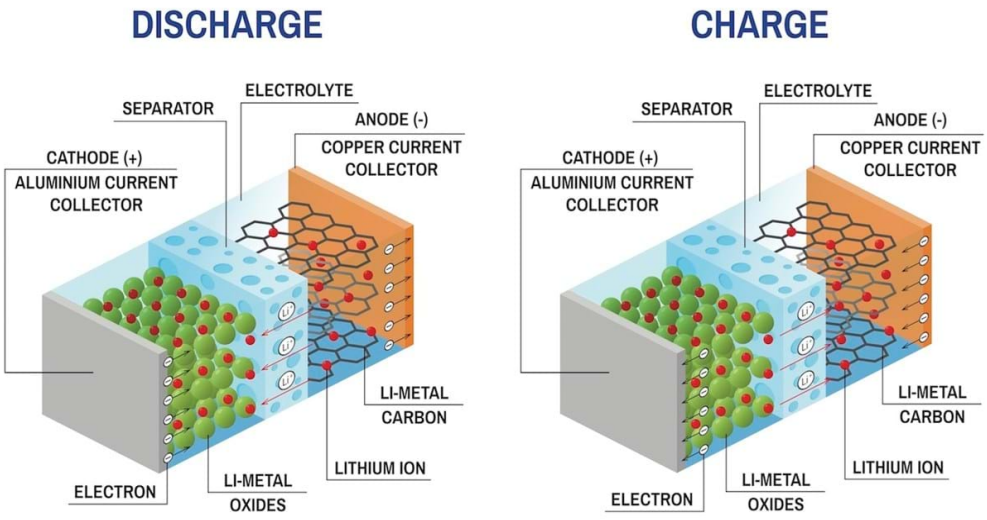

Figure 2.1: Lithium-ion battery circuit diagram

2.2 Li-ion battery terminologies

State of Charge, SoC

The state of charge is an estimation of the capacity within the battery pack at a particular time and is the ratio of the remaining capacity Q and the nominal capacity Q_n. The capacity of a cell is quantified in terms of Ampere hour (Ah), and the SoC is expressed as a percentage. SoC depends on the current, voltage and temperature and can be estimated by various methods. The SoC is given by:

$$SoC(t) = Q(t)/Q_n(t) \tag{2.1}$$

The methods for estimating SoC are done using Coulomb counting (calculated by the integrated current balance divided by the actual capacity of the battery cell) or using an OCV-SoC lookup table. An accurate estimation of the SoC can be obtained using recursive methods that take into account the non-linear behaviour of a Li-ion cell, like Kalman filters or Recursive Least Squares (RLS).

Open Circuit Voltage, OCV

This is the electric potential difference between the terminals of a battery when no load is connected across it. The OCV and SoC share a non-linear relationship with each other. The OCV and SoC are non-linearly related. The terminal voltage of the cell decreases non-linearly with the state of Charge. There is a difference between the terminal voltage and the SoC during the charging and discharging processes due to a phenomenon called hysteresis.

The cell potential is another term usually used in model-based simulations involving charge transfer physics and is defined as the sum of the cell OCV, the ohmic overpotential, the activation overpotential and the the concentration overpotential.

2.3 Li-ion battery faults

Different faults in a Li-ion battery can at times lead to uncontrollable states. To mitigate these faults, different techniques to detect and isolate them are being studied and used. The modelling and development of fault algorithms based on the type of faults can be divided into internal battery faults and external battery faults[4; 5].

Faults occurring internally

This type of fault is observed in the internal structure of the cell. These types of faults are the most critical ones as they could lead to various side reactions, some resulting in accelerated degradation and other faults which could cause serious damage. These reactions result in both electrical and mechanical abuse leading to electrolyte leakage. This thesis will focus on the internal battery faults as they are

more dangerous and are more likely to occur in a Li-ion battery than other faults and can be more harmful [6].

Overcharge occurs when the Li-ion cells' capacity varies or due to incorrect measurement of voltage and current or due to wrong SoC estimation [7]. Overcharge can cause unwanted electrochemical reactions in the cell and can damage the active materials and further lead to accelerated degradation and thermal runaway. If there is a development of a thick SEI layer,it could also lead to an ISC and could cause fires.

Overdischarge is caused by similar reasons as overcharge [7] and can decrease the overall battery lifetimes can be used and decrease temperature variation in the cell. It could also lead to swelling of the cell [8] and ISC [9].

Internal short circuit is a fault caused due to the damage of the separating layer between the electrodes. This fault can cause penetration of separator layer and leads to thermal runaway. Thermal runaway happens due to temperature buildup, mechanical deformation of the cell, formation of dendrites etc, [10; 11; 12]. ISC is one of the most common types of battery faults that leads to thermal runaway [23]. If there is a damage in the separator, then there will be contacts between the cathode and anode. Due to this interaction, the electrolyte in the cell starts an exothermic reaction, releasing heat. This can lead to buildup of heat over time and eventually cause thermal runaway [13]. The heat generated by this fault evolves into an uncontrollable state of thermal reactions aided by the decrease in cell resistance. [14]. There can be abnormal heat generation in the cell due to the internal battery faults and other side reactions, which further increases the battery temperature.

External short circuit fault happens when the cell tabs are connected by a low resistance path [15]. The ESC fault happens when an element capable of conducting heat and electricity comes in contact with both the cathode and the anode at the same time or due to side reactions.

Overheating can happen whenever an ISC or ESC happens [16] and chain reactions during it. The overheating fault can bring down the lifespan and capacity of the battery because it encourages SEI growth at the anode. This fault can also cause TR due to the heat inside the cell being unable to be released as fast as it is generated [17].

Accelerated degradation occurs due to cell aging and self-discharge which results in shorter lifespan. They can occur due to corrosion in current collectors or some changes in the electrode material. These faults cause thermal runaway where the high temperature and pressure will make the electrode reaction rate faster making the battery temperature even higher leading to possible explosion and releasing of toxic gases. They can also cause loss of cathodic active material and results in disintegration of the cell.

Thermal Runaway is caused by all the above specified internal battery faults and

is the most severe fault that can occur in a battery system. During TR, the battery can go into an uncontrollable state with enormous amount of heat being developed and even explosion and fires. The below figure explains the progression of thermal runaway in a lithium ion battery. TR happens due to many exothermic reactions, of which the decomposition of the SEI layer can release a large amount of heat. Further increase in temperature can take place due to the phase transitioned release of oxygen, which is consumed by the lithiated anode. When the temperature is close to the melting point of metallic lithium, it becomes very dangerous. These exothermic reactions also results in buildup of pressure inside the cell which can lead to rupture, releasing toxic gases [18]. A flowchart showing how thermal runaway develops in Li-ion cells [3] is shown below.

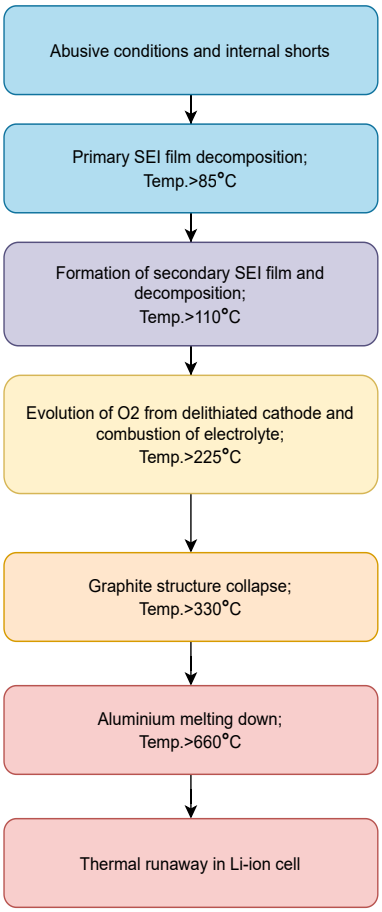

Figure 2.2: Flowchart showing how thermal runaway develops in Li-ion cells

Faults occurring externally

This type of fault occurs due to sensor faults, cooling system fault or a cell connection fault. These faults can also trigger any of the above internal battery faults.

Sensor faults occur in the main sensors used to measure the cell states in a LIB

which are the current, temperature and voltage sensors.They help monitor the cell states and help the Battery Management system (BMS) in keeping the battery's functionalities in check. Sensor faults can happen due to vibration and collision and other such instances [19]. These faults can also degrade the battery quickly and lower its performance.

A current sensor fault gives rise to incorrect SoC estimations. A voltage sensor fault can cause overcharge or overdischarge leading to wrong SoC and State of Health (SoH) estimations.A temperature sensor fault can cause the thermal management in the BMS to fail and lead to overheating, aging, capacity fade and short circuits.

Cooling System faults happen when either the motor or fan used by the cooling system for the battery fails due to the breakdown of the temperature sensor, wiring problems or a blown fuse [20; 21]. This system takes care of the cooling of the battery to maintain it within its operating range and if it fails, the heat is not transfers away from the battery leading to overheating and eventually thermal runaway.

Cell Connection faults occur when there is an improper connection between the cell terminals due to manufacturing defects, vibration or corrosion [22]. The cell resistance can increase rapidly due to this fault and overheat the cell or create imbalance to create an ESC or TR.

A BMS should be able to handle the above mentioned faults, along with its main functions (Measuring I,V,T, estimating SoC and SoH, thermal management, balancing etc.,) in an effective manner and prevent hazards. For complex faults, sometimes other safety measures like sensors and contactors might not be sufficient. This calls for fault diagnostic algorithms to be developed which can help detect and provide required control actions for these faults quickly.

2.4 Li-ion cell modelling

There are different ways to model a cell based on the operational physics of a cell and dynamics involved inside it. This thesis will focus on the aspect of cell modelling based on circuits that are electrically analogous to map the observed changes to the cell voltage under the influence of an input current. Since the equations formed and models are equivalent to what happens inside a lithium-ion battery cell, they are called as Equivalent Circuit Models (ECM). These models are simple to be understood, yet encompass most internal processes in a cell making them suitable for our use instead of the more challenging physics methods.

2.4.1 Equivalent Circuit Model of healthy Lithium-ion cells

The ECM of a healthy cell as mentioned in literature consists of:
Open-circuit voltage is the cause of a cell having a terminal voltage present across its terminals when a load is connected. When there is no load it is termed as the open-circuit voltage and it depends on the State of Charge of the cell. This rela-

tionship also involves temperature and can be modelled as a voltage source.

Equivalent series resistance(ESR) given by R_0 is the resistance in series with the voltage source that denotes the increase and decrease in the terminal voltage in reference to the open-circuit voltage during the charging and discharging processes. R_0 in the ECM denotes the resistance present in the electrodes, electrolyte, current collector and separator. The value of R_0 is a function of the cell's internal temperature and the SoC.

A current passes through the cell whenever the terminal voltage changes with respect to the OCV and causes a voltage drop. This is called polarization which becomes evident when a cell is put through a discharge pulse test characterized by a drop in voltage and when the current is applied during the pulse test and recovery when current is removed. Then, a slow diffusion process occurs leading to a voltage recovery that pits the terminal voltage at a value lower than the open circuit voltage. This dynamic behaviour can be modelled using one or more *resistor-capacitor sub-circuits* (or links) and is termed as a first order equivalent circuit model if one R_1-C_1 sub-circuit is used [2]. R_1-C_1 in the ECM represents the charge transfer process of the anode and cathode. In a 2-RC ECM, R_2-C_2 denote the diffusion processes of the cell. A combination of the OCV, R_0, R_1-C_1 link as per the above description gives us the ECM of a healthy cell as shown in Fig. 2.3.

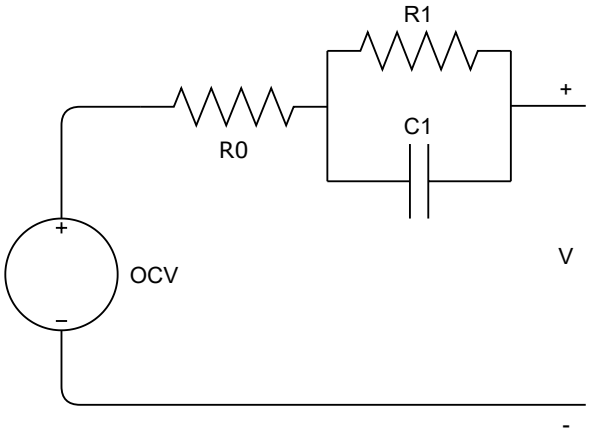

Figure 2.3: First order ECM of a healthy cell

2.4.2 Thevenin Model of Lithium-ion Cells with Internal Short Circuit faults

The effect of internal short circuit (ISCr) in a cell can be modelled using a short circuit resistance, R_{ISCr} connected in parallel to the terminals of the cell model. This ECM can be used to indicate internal short circuit as well as an external short circuit (ESCr) since both the faults have nearly same electrical performance [1]. This is shown in Fig. 2.4.

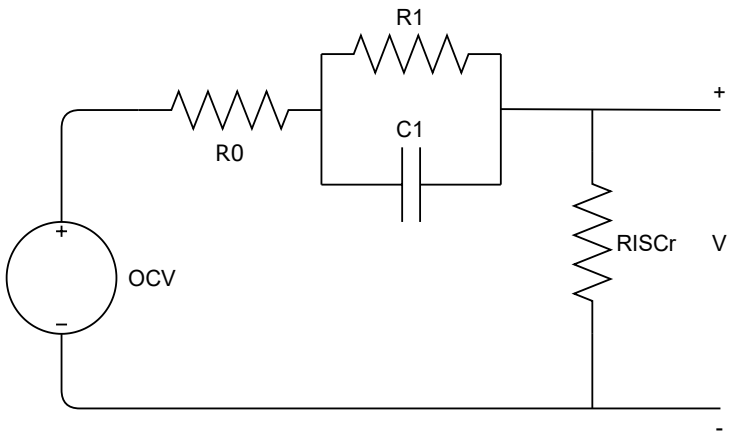

Figure 2.4: Thevenin ECM of a faulty cell

Different types of short circuit failures can occur. A *Hard short circuit* leads to extremely high magnitudes of current to be discharged through the cell making it an act like an actual resistor is placed in the circuit. This completely discharges and at the same time damages the cell. Hard short circuit resistances have magnitudes in mΩ leading to very fast thermal activity and rendering their detection futile since very little time remains for isolation and counter measures. *Soft short circuit* occurs at localized contacts between the anode and cathode and occur during the beginning of ISC. When internal short circuit occurs, it is characterized by a self-discharge current in addition to the load current. The self-discharge current leads to a drop in the OCV, SoC and rapidly decreases the terminal voltage.The soft short circuit resistances have resistances in terms of Ω thereby rendering the detection of soft shorts practical for detection, isolation and prevention [1].

2.5 Importance of Internal Short Circuit Fault Detection

Lithium ion batteries are being adopted rapidly in the electric vehicle industry due their superior energy density and efficiency. But safety of these systems is of utmost critical importance since faults like internal short circuit being the most common one leading to thermal runaway. The internal short circuit is the most common type of fault [23] leading to thermal runaway due to low internal short circuit resistance (in certain scenarios) leading to high short circuit current and temperature in the cells, all of which eventually leads to thermal runaway. Some examples of accidents due to internal short circuits are the Japan Airlines Boeing 787-8, JA829J aircraft fire [29] and the Tesla accident in 2013 [30]. Hence the detection of internal short circuits in Lithium ion battery systems is very important. In this thesis, the detection of internal short circuit has been performed using the rise in cell currents and temperatures as well as decrease in cell OCVs as a basis for detecting internal short circuits. In the FMU model, an ISCr detection method by obtaining the cell OCVs' threshold and their respective currents has been implemented.

2.6 Types of internal short circuit

As discussed in the previous section, the safety of a Li-ion battery is of utmost importance and detecting an internal short circuit, which is one of the most common type of fault is crucial to this. But there are varying intensities of an internal short circuit possible in a lithium ion cell and the following four short-circuit scenarios are most probable: (a) the short between the two current collectors, Copper and Aluminium (Cu-Al), (b) the short between the copper current collector and the cathode active material (Cu-Ca), (c) the short between the aluminium current collector and the anode material (Al-An), (d) the short between the active materials of the anode and cathode (An-Ca)

In [26], the expected electrical resistance of the various scenarios is calculated. But since the model used in the research and experimentation of the paper deals with a physical model with the different interfaces considered, the expected resistance is quite low for the Cu-Al scenario and high for the Al-An case. As the model used in this thesis does not consider all physical characteristics and material properties of a cell, it was decided to choose a lower resistance for the Al-An case and higher resistance for the Cu-Al case. This was done keeping in mind the real case outcomes and to emphasise the thermal behaviours which occur during these two cases. An overview of these cases and the respective thermal performances are presented in [27]. According to [28], the Cu-Ca and An-Ca cases will have limited, localized heating and Al-Cu will have homogeneous heating throughout the cell. Since the Lumped Battery Model used in the COMSOL simulation has the option of only giving the short circuit conductance as an input, the input short circuit conductance values for each case is the inverse of the expected resistances.

(i) **Copper-Aluminium (Cu-Al) short**: This short-circuit scenario between the two cell current collectors is the same observed when connecting a low resistance externally across the cell. During this scenario, the temperature rise usually observed is around 100°C.This temperature rise is limited since both copper and aluminium are good conductors of heat, but the energy due to this fault can be high because of the low resistances offered by these materials. Initially, the temperature rise is observed to be high, but it falls with increasing time.

(ii) **Copper-Cathode (Cu-Ca) short**: The active material in cathode is worst conductors of all components used in a Lithium ion cell. Hence, the short circuit current for this case is less and so is the temperature rise. Due to lesser SC current and temperature rise, the chances of side reactions are minimal in this scenario.

(iii) **Aluminum-Anode (Al-An) short**: This type of short is one of the most dangerous scenarios and can potentially lead to thermal runaway. The factors that make it so are: The anode's low electrical resistivity and high conductivity which could lead to a high power short; low temperature at which the reactions start at

the anode side; the low heat conductivity of this scenario leads to high localized temperature. As a consequence of these factors, the short circuit current and the temperature rise observed in this scenario are very high.

(iv) **Anode-Cathode short**: This is one of the most commonly observed fault scenarios in a Li-ion cell.The cathode's low material conductivity in this scenario leads to a lesser short circuit current value, but the temperature rises to a significant value due to the anode's poor thermal conductivity.

3

Methods

3.1 Fault detection simulation methods

One of the important functions of Battery Management System (BMS) present in a lithium-ion battery pack is to detect, diagnose the type and severity of the faults. Based on the operational limits and features such as sensors for voltage, current, temperature etc. added to ensure the battery pack's safety, the BMS takes suitable fault-tolerant control actions. This offers control for the users in detecting faults early and ensures reliable and efficient operation of the battery pack.

There are a number of fault diagnostic methods which can be broadly classified into Non-model-based methods and Model based methods. Non-model based methods use signal processing and battery data collection for fault detection. Though this kind of fault diagnosis improves accuracy, the computational cost is high and the large amount of data required for fault detection might not be always present with the designer. Model-based methods for fault diagnosis make use of electrical, thermal, electrochemical or a combination of these battery models. The main advantages of model-based methods is that they are simple, computationally less intensive and cost-efficient. Owing to these advantages, this thesis makes use of the model-based fault detection method using a co-simulation between COMSOL Multiphysics and Simulink. The first step is to design a vehicle model for various drive cycles in Simulink in order to obtain the input to the COMSOL battery model. After this, the outputs from the COMSOL model are analyzed in a co-simulated model in Simulink for fault detection using different mock-up units obtained by running the COMSOL model for different drive cycles and internal short circuit resistances. An easier explanation is provided by the illustration in Fig.3.1.

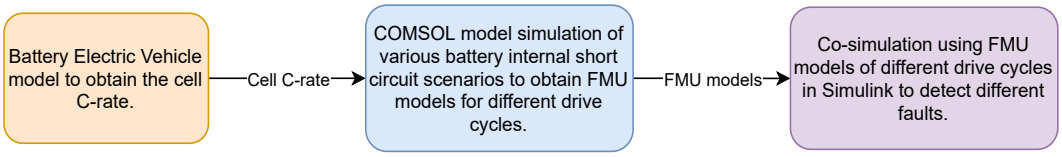

Figure 3.1: Process followed for fault detection

3.2 Electric Vehicle Simulink Simulation

A Battery Electric Vehicle (BEV) model contains an electric powertrain model with a Li-ion battery pack which acts as the source of electrical energy required to supply the required power to the electric motor and ultimately to the wheels to drive the vehicle. This is done based on the driveline model inputs like motor torque, brake force, vehicle speed and the driveline model outputs like the tractive force and the motor speed etc. Power losses account for the losses associated with each component and render an understanding of the power flow through the vehicle. A simple and effective model can be developed using the equation-based modelling approach in Simulink.

The BEV model begins by defining the vehicle dynamics (as a point-mass) of the system based on a free-body diagram as shown below. The tractive force has to overcome the aerodynamic drag, inertia (product of mass and acceleration), the grade force (if on a plane or on an incline) and the rolling resistance forces when the vehicle is defined to be moving forward in a positive direction. It can be described as follows:

$$F_{tr} = F_{aero} + ma + F_{grade} + F_{rr} \tag{3.1}$$

where F_{tr}, the total tractive force is the sum of the forces acting on the vehicle trying to increase the vehicle speed, m is the total mass of the powertrain that needs to accelerate, a is the acceleration.
F_{aero} is the aerodynamic drag force experienced by the vehicle when it is driving, due to the air flow through and around it. It can be expressed as:

$$F_{aero} = \frac{1}{2}\rho C_d A_f V^2 \tag{3.2}$$

where ρ is the air density, C_d is the aerodynamic drag coefficient, A_f is the effective vehicle cross-sectional area, V is the vehicle speed.
From equation (3.1), F_{grade} can be defined as the force acting on the vehicle's gravitational force which is in parallel with the road when travelling uphill or downhill. It can be described as:

$$F_{grade} = mg \cdot sin(\theta) \tag{3.3}$$

where g is the gravitational constant, θ is the angle between the road and the horizontal plane.
Again from (3.1), F_{rr} can be defined as the rolling resistance force caused by the vehicle's tyres during rolling. It can be described as:

$$F_{rr} = mgC_{rr} \tag{3.4}$$

where C_{rr} is the rolling resistance coefficient.
A simple PID controller acts as the driver system and the reference speed to the model is provided by the drive cycle in order to analyze the powertrain load levels and the energy consumption. The error between the output of the vehicle dynamics block and the driver system determines the tractive force input to the vehicle dynamics. The tractive force is subtracted from the resistive forces as mentioned above

and divided by the total mass factor to result in the vehicle acceleration. On double integrating the acceleration, we obtain the velocity and displacement or position of the vehicle. The product of the tractive force and the velocity results in the tractive power which upon integration gives the total tractive energy needed.
For the motor system inside the vehicle model, we first compute the motor's mechanical output power given by:

$$P_{mot} = T_{mot}\omega_{mot} \tag{3.5}$$

where T_{mot} is the motor torque and ω_{mot} is the rotational speed. The power losses can be characterized as a polynomial equation as:

$$P_{loss} = k_c T^2 + k_i\omega + k_\omega\omega^3 + C \tag{3.6}$$

where k_c, k_i, k_w and C are motor loss constants. The input power would be the sum of the power output and the losses.

$$P_{in} = P_{mot} + P_{loss} \tag{3.7}$$

Additionally, the propelling and regeneration efficiencies can be calculated from the results of the input and output motor powers respectively.
The battery can be modelled by considering only the internal resistance, R_{int} of the cell along with a the OCV modelled as a voltage source supplying a load, R_{load}. In this thesis, we consider the parameters presented in the table below during the battery electric vehicle simulation.

Table 3.1: Parameters used during BEV simulation

Parameter	**Value**
Gross vehicle mass (m)	2500 kg
Aerodynamic drag coefficient (C_d)	0.38
Air density (ρ)	1.23 kg/m^3
Battery capacity	66 kWh
Vehicle frontal area (A_f)	2.1 m^2
Gravitational constant (g)	9.81 m^2
Inclination angle (θ)	0°
Initial SoC	0.95
Battery voltage	350 V
Rolling resistance coefficient	0.01
Wheel radius	340 mm
Motor loss constant (k_c)	0.12 s/kgm^2
Motor loss constant (k_i)	0.01 J
Motor loss constant (k_ω)	1.2e^{-5} kgm^2
Motor loss constant (C)	600 W

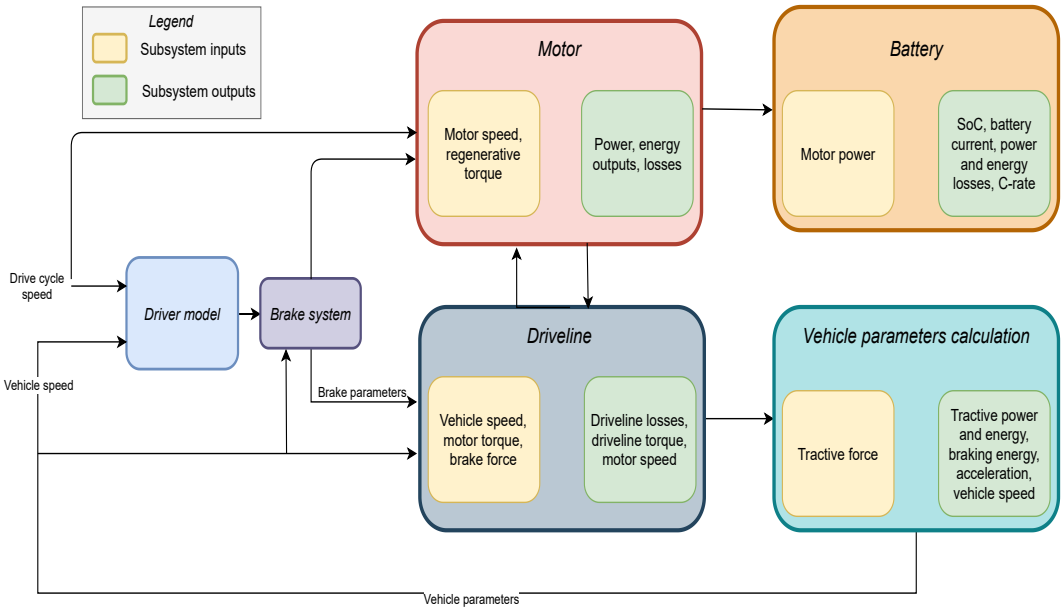

Figure 3.2: Schematic representation of BEV simulation to obtain the cell C-rate.

The output of the simulation which is the cell C-rate is given by:

$$C - rate = \frac{Discharge\ (or\ charge)\ current}{Rated\ capacity} \tag{3.8}$$

Drive cycle

Emission regulatory organizations have developed different drive cycles comprising the variation of reference speed over time. They are used to judge vehicle's driving performance according to the emissions and fuel economy. As explained in the previous section, the vehicle is affected by various parameters and the input to the BEV model's driver system are different drive cycles. First, a self-defined constant drive cycle (1200 seconds) as in Fig.3.3 is used to check if the model implementation is correct and to determine if the short circuit trigger at the specified time is working as it should. The model is then validated for the Worldwide Harmonised Light Vehicles Test Procedure (WLTP), which has a longer duration and can simulate an actual day-to-day driving scenario of a vehicle. The WLTP, shown in Fig.3.4 is a much more intense drive cycle and has can be used for most vehicle varieties. The WLTP also takes considers the CO_2 impact due to additional features in a vehicle.

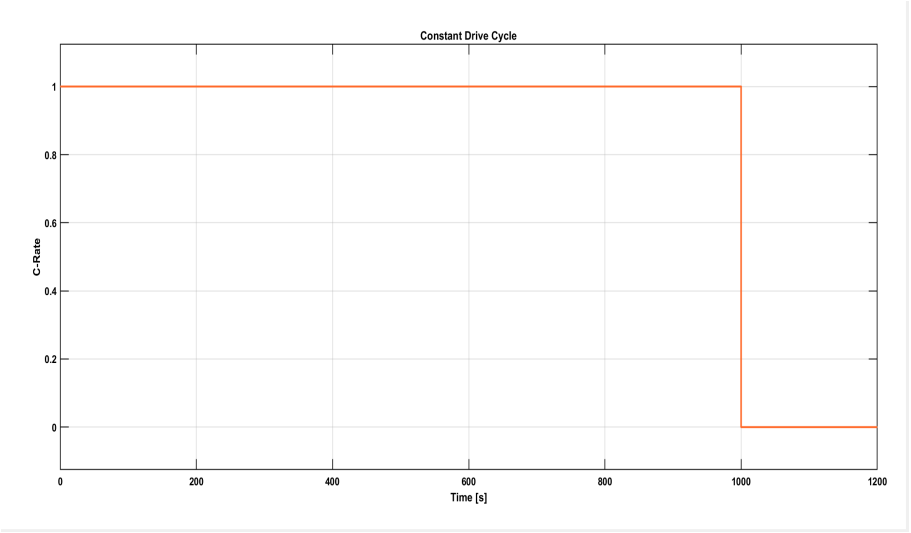

Figure 3.3: Drive cycle with constant C-rate

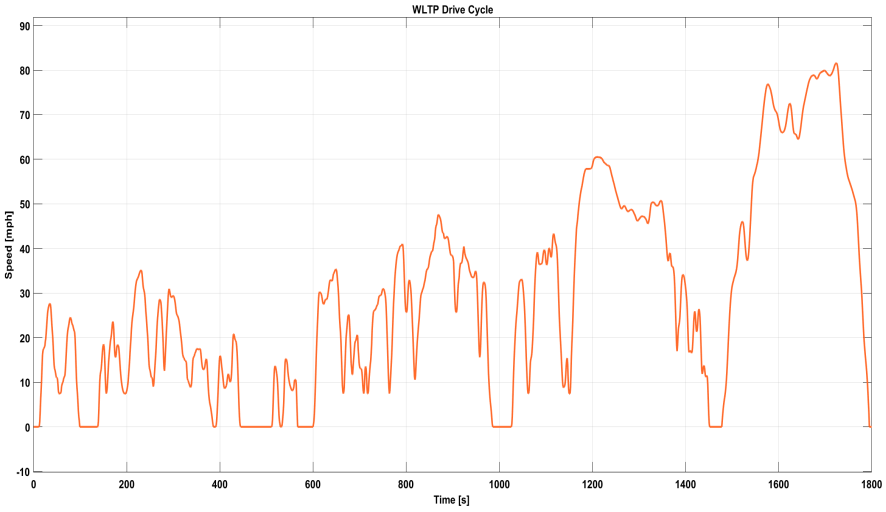

Figure 3.4: WLTP Drive Cycle

3.3 Lithium-ion Cell COMSOL Simulation

COMSOL Multiphysics is a general-purpose software based on advanced numerical methods with the ability to study various physics. It can be used to model the workflow completely from designing the geometry to post-processing and analysis of the results. Some of the advantages in using such software are that models can be processed through built-in or defined equations, parameters and materials for user-defined geometry can be defined in the add-on packages and the results can be analyzed in a time-bound and cost effective manner.
The procedure followed for the COMSOL simulation is:

1. We start by selecting a new 3D time-dependent study in the Model Wizard and choosing the *Lumped Battery* interface inside *Batteries* under the *Electrochemistry* physics. We also add the *Heat Transfer in Solids* physics for a *Multiphysics* simulation to analyze the temperature variation during the fault condition.
2. Then, we define the *Global Definitions* which are used during model development and the subsequent simulation process. In our case, they are defined in the *Global Definitions* tab. The first parameters to be given are the *Geometry Parameters* to define the shape of the 18650 type of cylindrical cell and some of them are presented in 3.2.

Table 3.2: Geometry Parameters used during COMSOL simulation

Parameter	**Value**
Battery diameter (d_{batt})	18.55 mm
Battery radius (r_{batt})	9.275 mm
Battery height (h_{batt})	65.25 mm
Battery terminal thickness (h_{term})	1 mm
Battery terminal radius (r_{term})	3 mm

The electrical parameters of the battery are defined separately as in 3.3 for the rechargeable Lithium-ion rechargeable cell Samsung INR18650-35E [24] taken as reference.

- Then the driving cycle C-rate for the cell obtained from the BEV model is given as an interpolation function, *Crate(t)* for all three drive cycle cases. This ensures that the defined battery model takes into account the changes in the cells' C-rate.
- A separate interpolation function, *Short(t)* is introduced to define when the internal short circuit must be triggered. For all three C-rate cycles, the internal short circuit is triggered at 600 seconds. We consider a case of high resistance for non-fault conditions and a very low resistance in

Table 3.3: Battery Parameters used during COMSOL simulation

Parameter	**Value**
C rate (C_{rate})	2
Cell capacity (Q_{cell})	3.35 Ah
1C current (I_{1C})	3.35 A
Reference temperature (T_0)	25°C (298.15 K)
Battery density (ρ_{batt})	2000 kg/m^3
Battery heat capacity (C_{pbatt})	1400 J/kgK
Heat transfer coefficient (h_t)	30 W/m^{2}K
Initial temperature (T_{init})	25°C (298.15 K)
Internal short circuit conductance (G_{short})	(*Varies based on the type of ISCr*)

case of the different kinds internal short circuit faults. Since COMSOL considers these values in terms of conductance, they are defined as G_{short} in the triggering cycle definition presented in the table below.

3. The applied current variable for the battery model is defined in the *Component Definitions* as:

$$I_{app} = I_{1C} * driving(t) \tag{3.9}$$

Another variable, G_{cycle} is defined for the short circuit trigger cycle, *Short(t)*. The SoC-OCV curve is then defined as a separate interpolated variable, E_{OCP}. The data is referred from an earlier thesis and was provided to us by our academic supervisor.

4. The geometry is of the battery model is defined in the *Geometry* tab. Cylinders with the specified cell height and cell radius denote the cell and additional cylinders with the specified terminal dimensions denote the cell terminals. This is repeated to design 3 cells using the *Array* function. The cells are connected using independent connectors which are designed using the *Block* function. The cells, air domain and connectors are assembled as separate entities using the *Explicit Selection* option. This array of 3 cells is mirrored once so as to get a configuration of 6s2p. The geometry is influenced by the *Lumped Li battery pack* example available in the COMSOL applications library.
5. Air is assigned as the material for the air domain surrounding the cells. Aluminium is used for the cell connectors and Active Battery material is used for the cells.
6. As described previously, the *Heat Transfer in Solids* and *Lumped battery* physics are opted for this multiphysics simulation.
   - The *Heat Transfer in Solids* physics block has the three cells and the connectors chosen as solids using the *Solids* domain . Using the *Heat Flux* boundary condition, the air domain is introduced with a convective heat flux element which follows the equation,

$$q_0 = h_t * (T_{init} - T) \tag{3.10}$$

     where q_0 is the rate of change of conductive heat flux.
   - In the *Lumped Battery Model* physics, we define the time-dependent *Cell Equilibrium Potential* which varies according to the SoC and the temperature. The cell's *Voltage Losses* which depend on the OCV, the activation potential and other factors are also defined here. This is repeated for all three cells.
7. *Electrochemical Heating* is chosen as the Multiphysics option for the individual cells by coupling the *Lumped Battery* and *Heat Transfer in Solids* physics interfaces.
8. A physics controlled mesh and a coarse element size are chosen so that the complexity and time taken for the study to run is minimized.
9. The *Time Dependent study* is run for 1200 seconds for the constant drive cycle and 1800 seconds for the WLTP cycle. This processes the multiphysics model with a 10 second interval between each time step to display the results.

3.4 Electric Vehicle and Lithium-ion Cell Co-simulation

After obtaining the results, we derive the Functional Mock-up Unit (FMU) model of the COMSOL simulation. This COMSOL Multiphysics simulation is integrated into Simulink for further analysis and fault detection using the *Livelink for Simulink* functionality. During the cosimulation, Simulink sends new input values to the COMSOL model and notifies that a simulation from t to $t + dt$ has to be performed. COMSOL finds consistent initial conditions based on the changed input parameter values and performs the simulation. COMSOL sends output values from the model when the simulation of the communication step has been completed [25]. Before setting up the COMSOL model for cosimulation, it is important to understand that the study is allowed to contain one time-dependent or stationary study step. It must also be made sure that the COMSOL model's units and the ones in Simulink match since there is no unit conversion check during the cosimulation. The process workflow for cosimulation is as follows:

1. Add the *Cosimulation for Simulink* node present under the *Study* tab. This can also be done by right-clicking on *Global Definitions* and selecting *Cosimulation for Simulink*.
2. Specify the inputs needed in order of their requirement in the COMSOL Cosimulation block in Simulink.In our case, we need the C-rate (C_{rate}) of the battery and the short circuit conductance (G_{short}) as input parameters. Initial values can also be entered here. In case new inputs are required, click on + and select one or more of the options from the drop-down list in the *Parameters* column.
3. As for outputs, we select the cell voltages, cell potentials, cell temperatures, cell currents and the short circuit current for further use in the cosimulation Simulink block. Select *Study 1* in the study section.
4. Save the COMSOL MPH file. Enter the file path and file name. Click on *Export* to generate the Functional Mockup Units (FMUs).

Fault detection using cosimulation

Once the cosimulation in Simulink is set up, it is important to validate if the model is working as intended. Another purpose of using the cosimulated environment is to test the detection of internal shorrt circuit fault along with overdischarge protection, undervoltage and BMS shutdown. The States of Charge of the faulted cell and normal cell are also estimated to lend us a better comparison between the two conditions. The process followed for the fault detection algorithm is as follows:

1. Open *COMSOL Multiphysics 5.6 with Simulink* and insert the COMSOL Cosimulation block. Enter the required FMU filename as per the drive cycle. The communication step is decided by the user and for this thesis it is 50 since it enables faster cosimulation without compromising the fault detection quality.
2. The main parameter used to check for detection is the cells' OCVs since it was found be more reliable (considering that the cells are not connected to any load) than the cell temperatures or the measure of the rate of change of the cell currents. Implement the undervoltage detection by comparing each cell

OCV with a slightly higher value than the datasheet specified value of 3.25V. If the detected OCV is lesser than or equal to this, the respective LED for the cell switches on inside the virtual fault detection dashboard for undervoltage fault.

3. Similarly, implement the logic for the overdischarge protection by comparing each cell OCV with a slightly higher value than the datasheet specified value of 3.10V. If the detected OCV is lesser than or equal to this, the respective LED for the cell switches on inside the virtual fault detection dashboard for overdischarge fault.
4. The internal short circuit fault detection is then implemented by assuming that the OCV for each cell is normally distributed and that the results can be analyzed using statistical methods. Considering the cell OCVs as the characteristic parameter and that the extreme values will be represented by cell 2 which has an internal short, we calculate the mean and standard deviation. This is done using the moving mean block in Simulink that moves over the data sample by sample, and the block computes the average over the data in the window. Similarly using the respective blocks in Simulink for moving standard deviation and moving minimum, they are calculated and used to identify the amount that the minimum deviates from the mean measured in terms of standard deviation units [1]. This is the negative significance, M_{neg} given by:

$$M_{neg} = \frac{X_{min} - \mu}{\sigma} \tag{3.11}$$

   This thesis deals with only the negative significance as the characteristic parameter (OCV) is never going in the positive direction once any fault is detected. M_{neg} is compared with a threshold value to decide if the cell corresponding to the minimum is in danger of being internally short circuited or not. This threshold is taken from (-4σ, ∞) since the 99.99% confidence interval makes the possibility of encountering an internal short around 0.007%, increasing the accuracy of the detection.
5. The final layer of protection applied is to shut down the BMS when the OCV decreases to a value below 3.05V. This ensures that the supply is cut-off and limits further damage to the cells. This is implemented in a similar way as the detection for the undervoltage fault and the overdischarge protection.
6. The cell SoCs are estimated using the Coulomb Counting method in the *SoC Estimation* block. The simple method to compute the SoCwhich follows the equation:

$$SoC(t) = SoC_0 + \frac{t}{Q_{nom}} \int_0^t i(t)\, dt \tag{3.12}$$

   where SoC_0 is the initial SoC is assumed as 0.7 and the nominal capacity, Q_{nom} is given as 3.35 Ah. The SoC estimation gives an idea of the SoCs at different stages of the co-simulation and the SoC once fault is detected or the SoC value just before the BMS is shutdown. A comparison of the normally functioning first cell and the internally shorted second cell is also shown.
7. Run the model by supplying the respective C-rates for each drive cycle. Any value of internal short circuit conductance can be given to check the fault conditions to the G_{short} port in the cosimulation block.

4

Results

The following part of the report deals with the results obtained during the fault simulation for the four types of internal short circuit conditions. This includes obtaining the cell C-rate using the BEV model simulation in Simulink followed by the COMSOL model simulation and FMU cosimulation in Simulink for Al-An and Cu-Ca type of internal short circuit faults for each drive cycle. Using these FMU models, the fault detection method is implemented by cosimulating COMSOL with Simulink.

4.1 Fault Detection with Constant Battery C-rate

This section presents the results obtained from the COMSOL simulation and the subsequent fault detection using cosimulation for drive cycle with constant C-rate.

4.1.1 Internal Short Circuit Detection with COMSOL Simulation (Constant C-rate)

The drive cycle for 1200s as in Fig.4.1 with a constant C-rate of 1 for 1000s was given as the input to the COMSOL model and subsequent cosimulated model in Simulink. This was done to verify the model's correctness along with the fault triggering mechanism and observe the results. Fig.4.2 is the SoC-OCV charging curve given to the COMSOL model for all ISCr conditions and is the same for all three drive cycles.

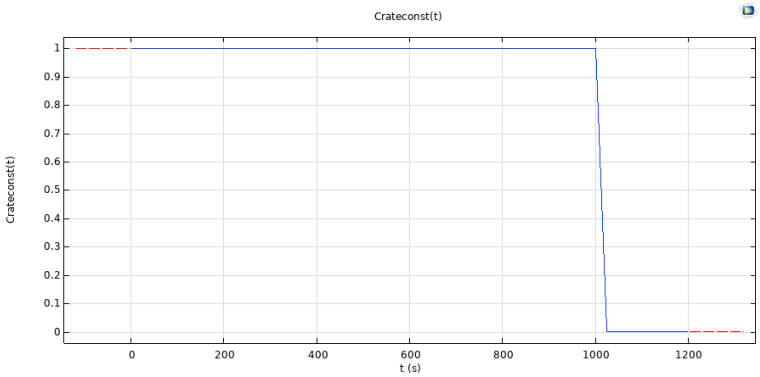

Figure 4.1: Drive cycle input with constant C-rate of 1

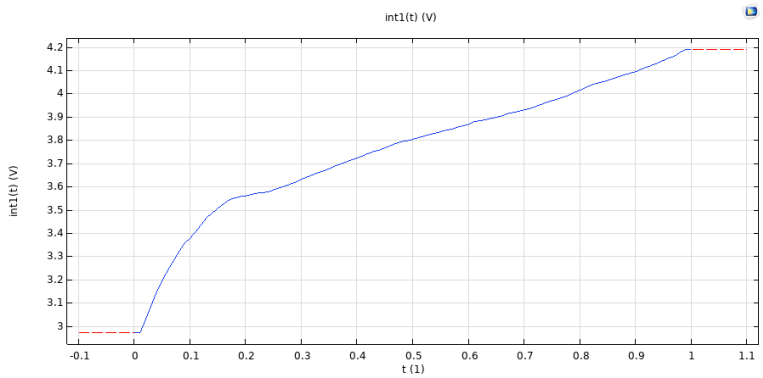

Figure 4.2: OCV-SoC input for cells

Al-An short

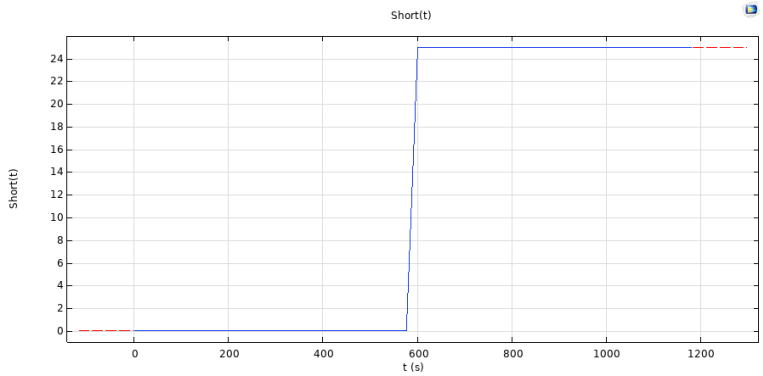

Figure 4.3: Al-An internal short circuit trigger cycle

Fig.4.3 shows the short circuit trigger cycle activating the Al-An internal short which has a conductance of 25S at 600s till the end of the drive cycle.

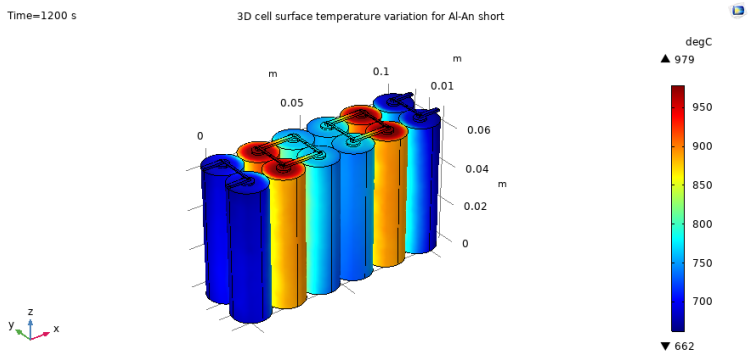

Figure 4.4: 3D cell surface temperature variation for Al-An short

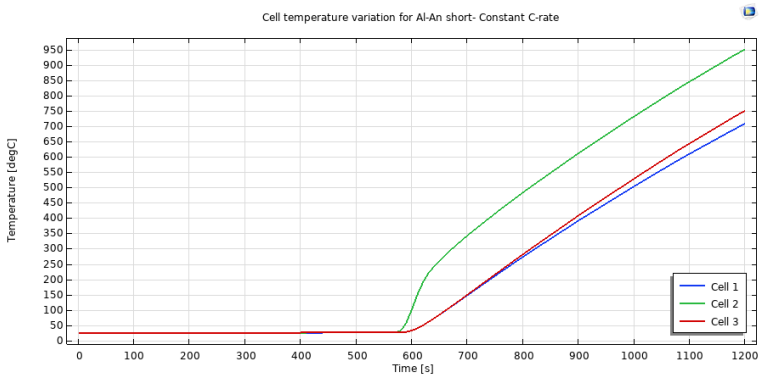

Figure 4.5: 1D Cell temperature variation for Al-An short

Fig.4.4 shows the surface temperature distribution over the three cells. The maximum temperature of 979°C can be seen at the internally shorted second cell while the first cell remains relatively at a lower temperature. The third cell, even though not undergoing any fault, is at a higher temperature than the first cell since it is influenced by the second cell's thermal activity as it is connected in series with it. Fig.4.5 shows the temperature distribution over the cells. It indicates the severity of the Al-An internal short circuit fault which is primarily due to it being a high power short owing to the low electrical resistivity offered by the anode.

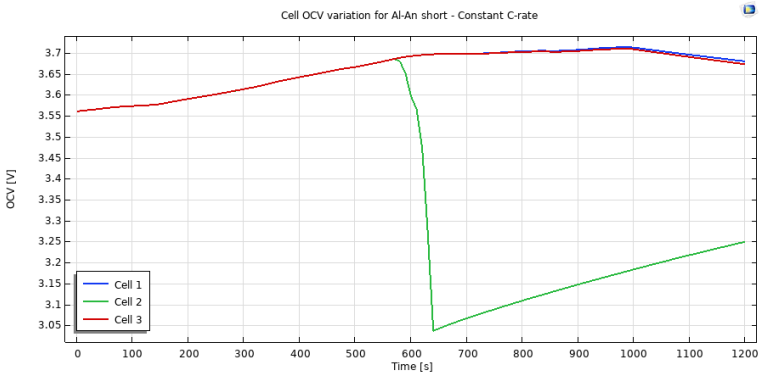

Figure 4.6: Cell OCV variation for Al-An short

Fig.4.6 presents the cell OCVs which is dependent on the cell SoC and the temperature. The plot shows that the difference between the shorted cell's OCV and the non-shorted cell is quite large due to the induced fault. As soon as the fault is triggered, the OCV of the second cell falls at a sharp rate and is accompanied with a high short circuit current, shown in the figure below.

Figure 4.7: Cell SoC variation for Al-An short

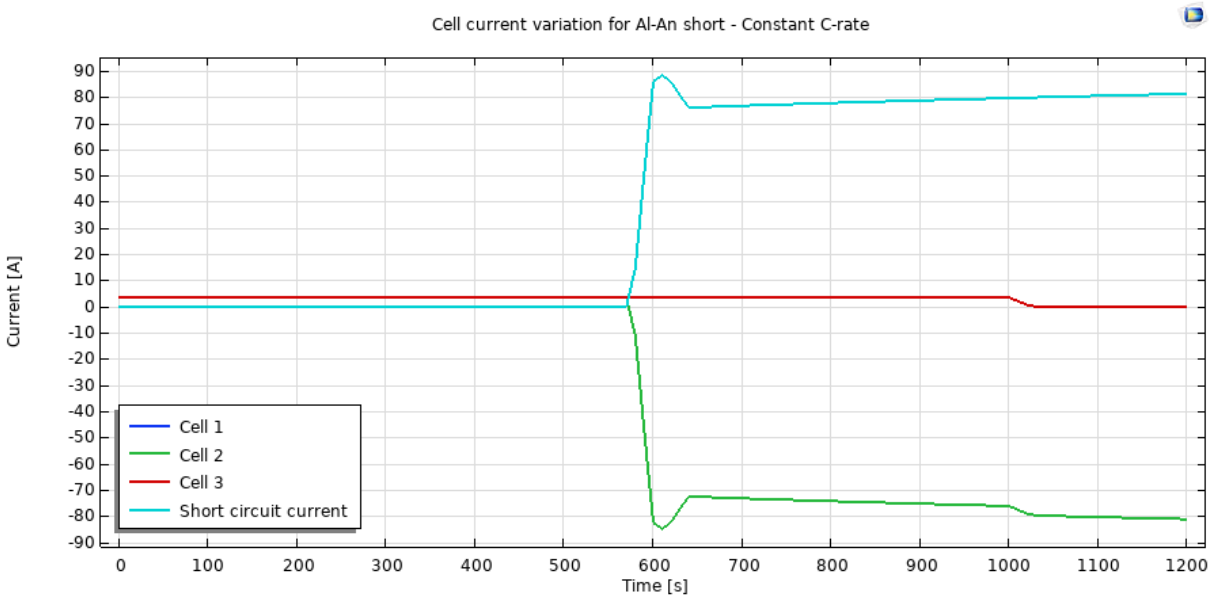

Figure 4.8: Cell current variation for Al-An short

Fig.4.7 shows the variation of the cell SoCs for the driving cycle with constant C-rate. It is evident that the cell discharges rapidly once the fault is triggered and the SoC also decreases at a fast rate. This is due to the rapid increase in discharge current as shown in Fig.4.8, where the short circuit fault current reaches close to 90A rendering the cell unstable in a very short span of time of around 30s. Since this ISC scenario has high thermal activity due to the anode's low very low electrical resistivity.

Cu-Ca short

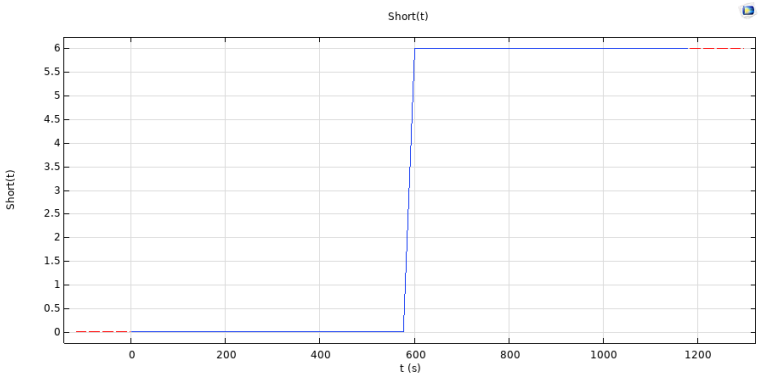

Figure 4.9: Cu-Ca internal short circuit trigger cycle

Fig.4.9 shows the short circuit trigger cycle triggering the Cu-Ca type of internal short circuit at 600s with a conductance of 6S.

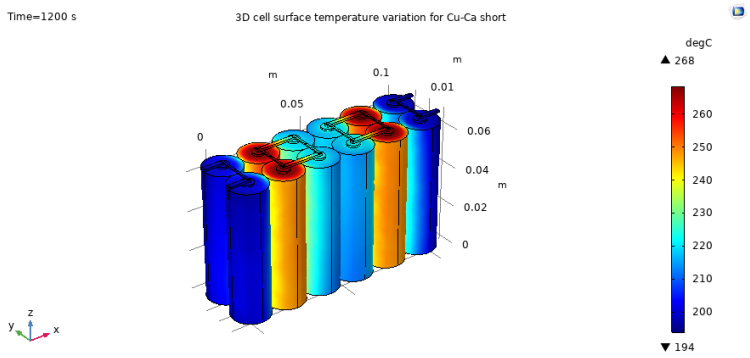

Figure 4.10: 3D cell surface temperature variation for Cu-Ca short

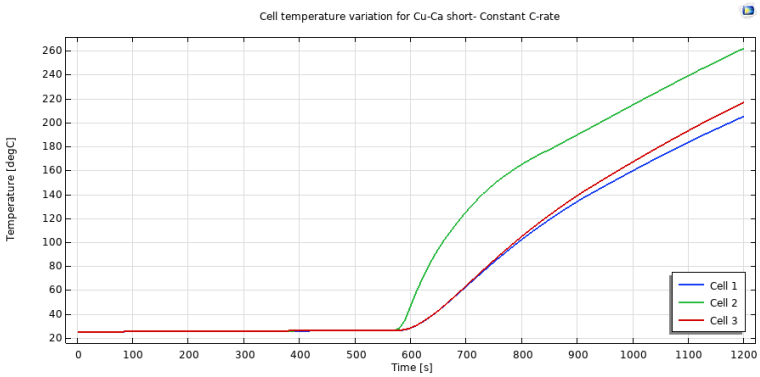

Figure 4.11: 1D Cell temperature variation for Cu-Ca short

Fig.4.10 shows the effect of the Cu-Ca internal short and is replicated in Fig.4.11 as well indicating that cell 2 temperature increases rapidly to a maximum of 268°C. This scenario is fairly infrequently observed in Li ion cells. The reason for the lower temperature rise is because the cathode material is a poor conductor of heat and consequently the heat released is not enough to trigger any further chemical reactions.

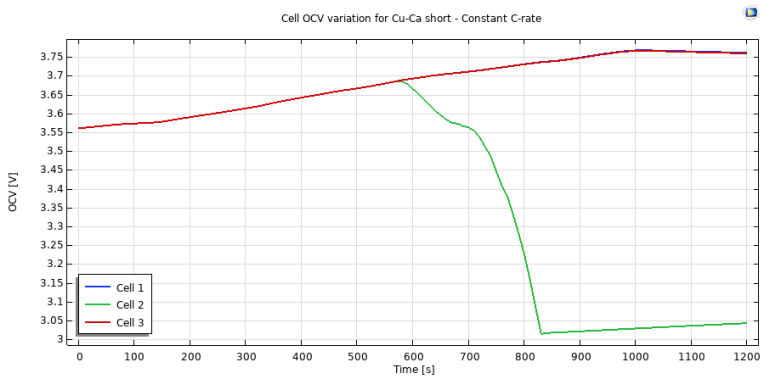

Figure 4.12: Cell OCV variation for Cu-Ca short

The OCVs of cells 1 and 3 as indicated in Fig.4.12 rise to a certain value around 3.75V and stabilizes as the drive cycle input becomes zero. It can be observed that the cell 3 OCV falls as soon as the fault is triggered but at a much slower rate as compared to the Al-An short because of the low short circuit conductance values.

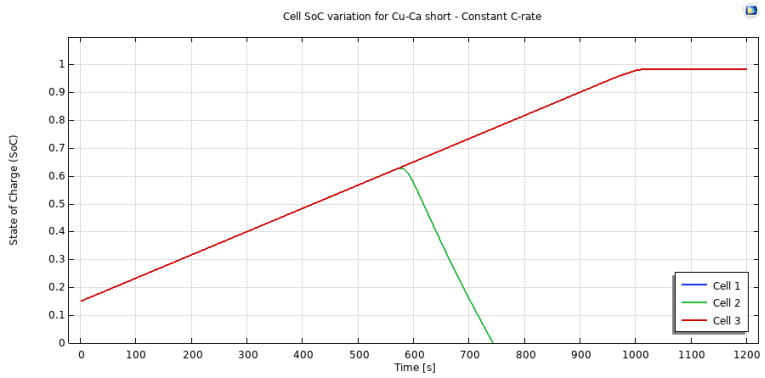

Figure 4.13: Cell SoC variation for Cu-Ca short

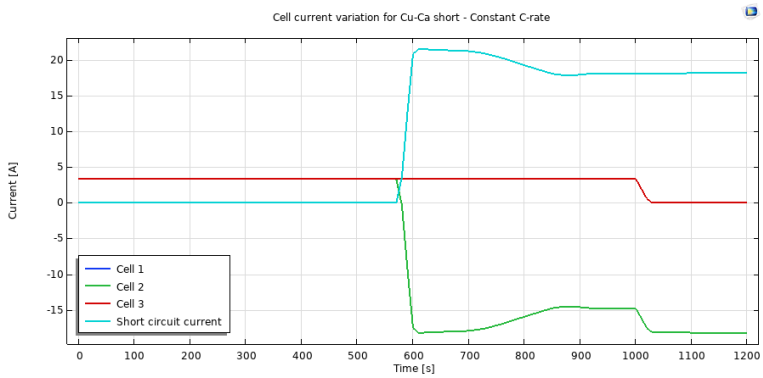

Figure 4.14: Cell current variation for Cu-Ca short

Fig.4.13 shows the state of charge variations for each cell before, during and after the fault. The SoC falls at a slower rate than the previous type of internal short circuit fault and this is evident due to the increase in discharge current displayed in Fig.4.14.

Cu-Al short

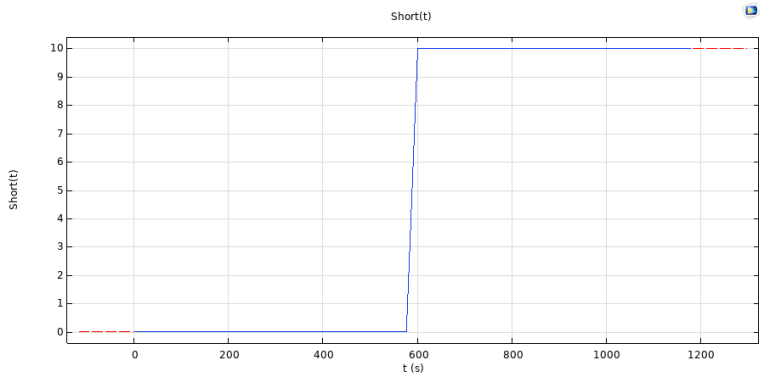

Figure 4.15: Cu-Al internal short circuit trigger cycle

Fig.4.15 shows the short circuit trigger cycle triggering the Cu-Al type of internal short circuit at 600s with a conductance of 10S. Fig.4.16 shows the effect of the Cu-Al internal short and is replicated in Fig.4.17 as well indicating that cell 2 temperature increases rapidly.

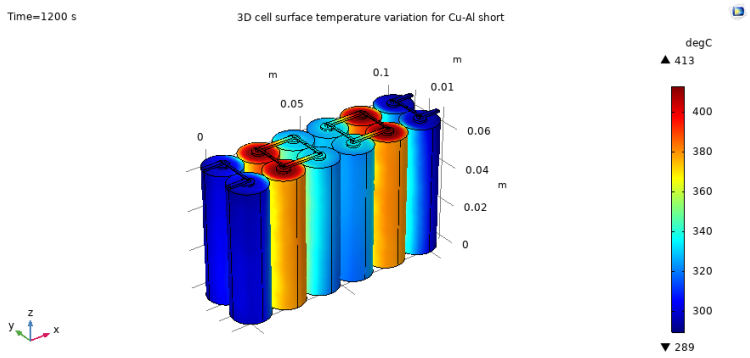

Figure 4.16: 3D cell surface temperature variation for Cu-Al short

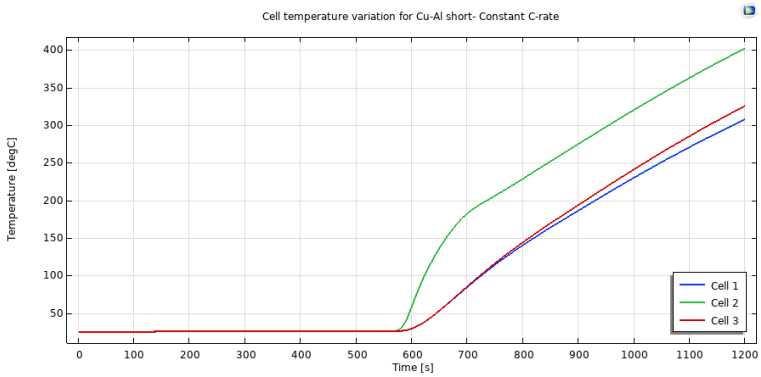

Figure 4.17: 1D Cell temperature variation for Cu-Al short

In this case for the Cu-Al short, the temperature rises to about 413°C. This is similar to the cell's terminals being externally connected with a low resistance path as evident from Fig.4.16. Fig.4.17 shows that though the temperature rises to a high value, the materials are good conductors of heat and hence can dissipate heat quickly.

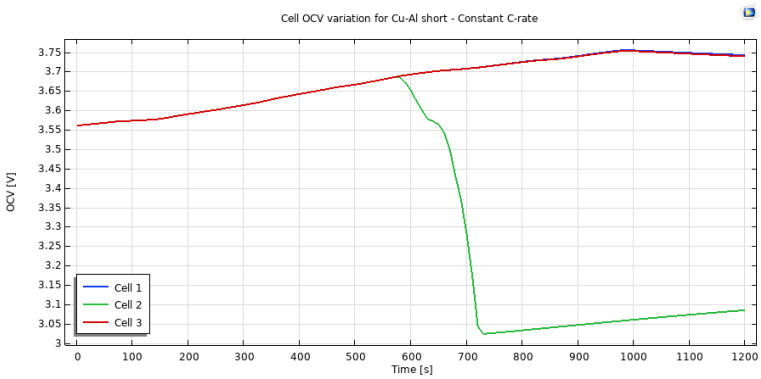

Figure 4.18: Cell OCV variation for Cu-Al short

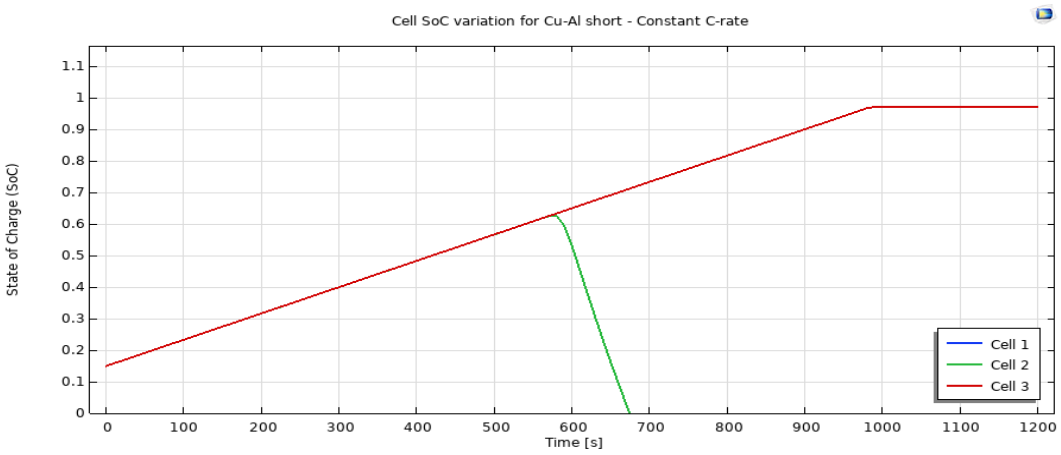

Figure 4.19: Cell SoC variation for Cu-Al short

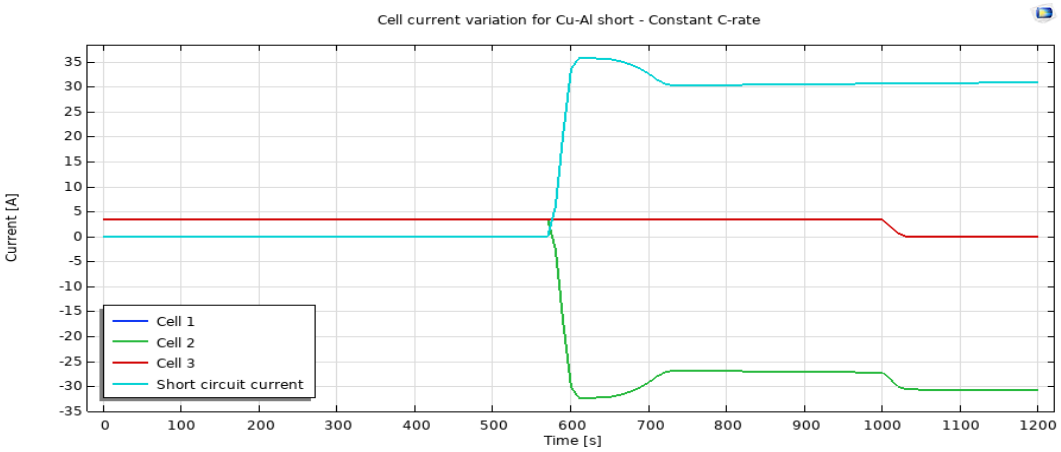

Figure 4.20: Cell current variation for Cu-Al short

The OCVs of cells 1 and 3 as indicated in Fig.4.18 rise to a certain value and stabilize as the drive cycle input becomes zero. Cell 2 OCV falls as soon as the fault is triggered at a quicker rate due to the larger short circuit conductance value. The SoC variations for each cell as seen in Fig.4.19 is much steeper for this case as short circuit current increases and the rapid fall of OCV. Cell current variations are shown in Fig.4.20 for this type of short. The cell short circuit current is around 35 A, but the temperature rise accompanying the current rise can lead to a thermal runaway scenario.

An-Ca short

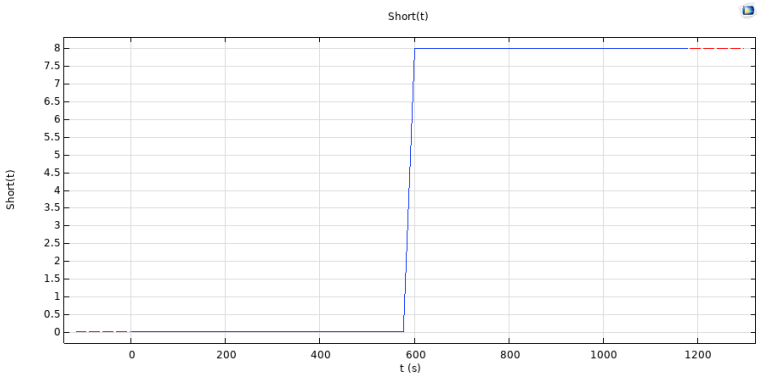

Figure 4.21: An-Ca internal short circuit trigger cycle

Fig.4.21 shows the short circuit trigger cycle activating the An-Ca internal short which has a conductance of 8S at 600 s till the end of the drive cycle at 1200s.

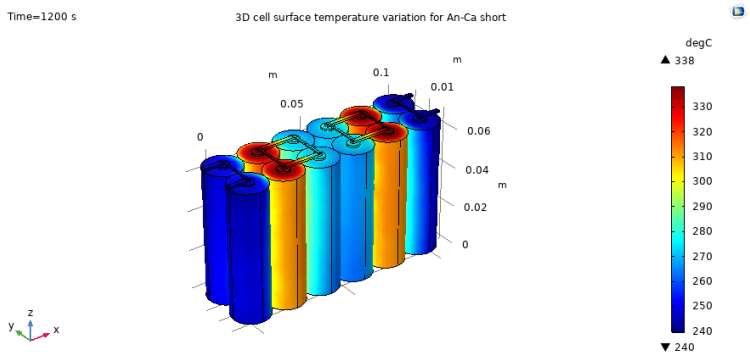

Figure 4.22: 3D cell surface temperature variation for An-Ca short

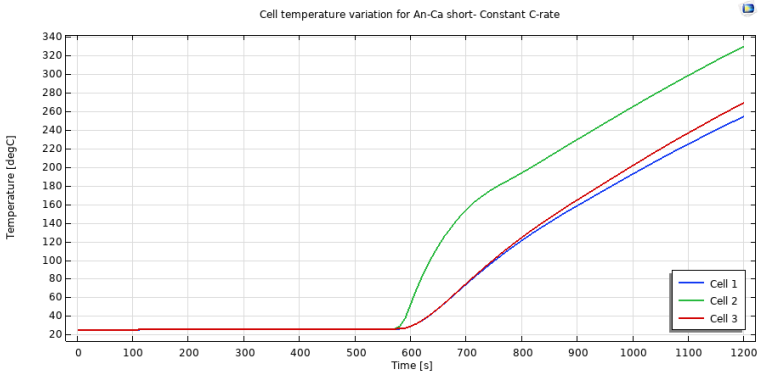

Figure 4.23: 1D Cell temperature variation for An-Ca short

In this case the temperature rises to about 340°C as evident from Fig.4.22. This is important and is commonly seen in the An-Ca short which is the most probable type of fault observed in Li ion cells. Fig.4.23 exhibits that the temperature rise is in between the observed temperature increases for the 25S and the 6S case. This is due to the cathode material's low conductivity and hence higher resistance (or lower conductance).

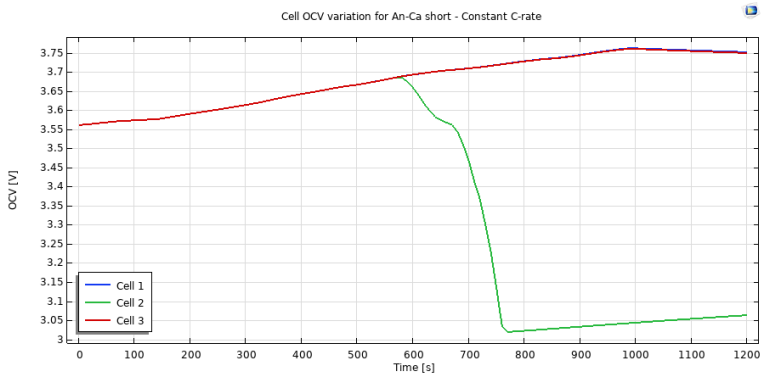

Figure 4.24: Cell OCV variation for An-Ca short

Fig.4.24 indicate that the OCVs of cells 1 and 3 as rise to a certain value and stabilize as the drive cycle input becomes zero. The cell 2 OCV falls as soon as the fault is triggered but at a slower rate compared to 10S case but faster than the 6S case.

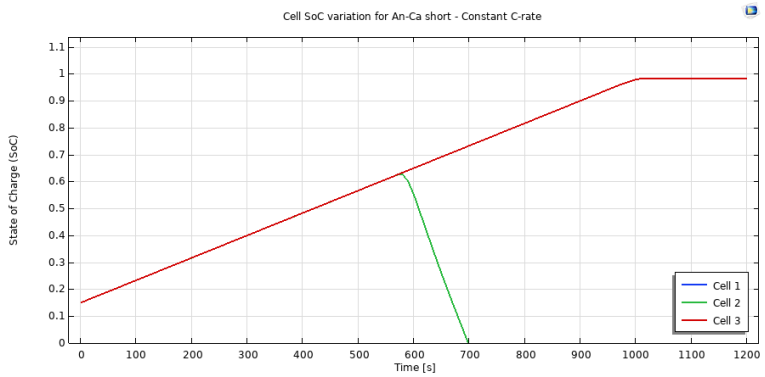

Figure 4.25: Cell SoC variation for An-Ca short

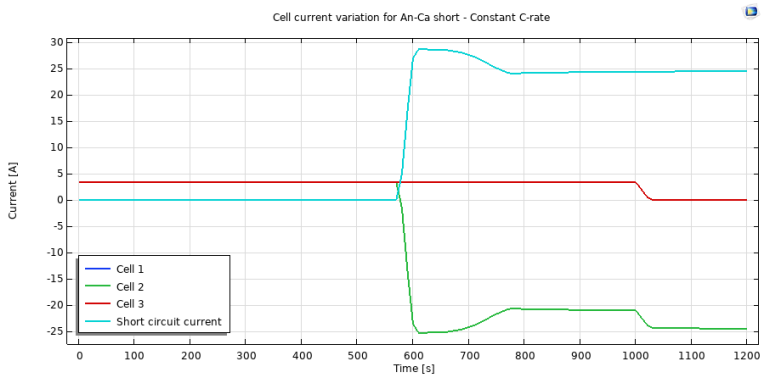

Figure 4.26: Cell current variation for An-Ca short

The State of Charge variations for each cell is much slower than the 10S case and is reflected in Fig.4.25 with the rise of the SC current and fall of OCV. The cell short circuit current is around 30 A, due to a higher resistance or lower conductance short than 10S case presented in Fig.4.26.

4.1.2 Internal Short Circuit Detection with Co-simulation (Constant C-rate)

Al-An short

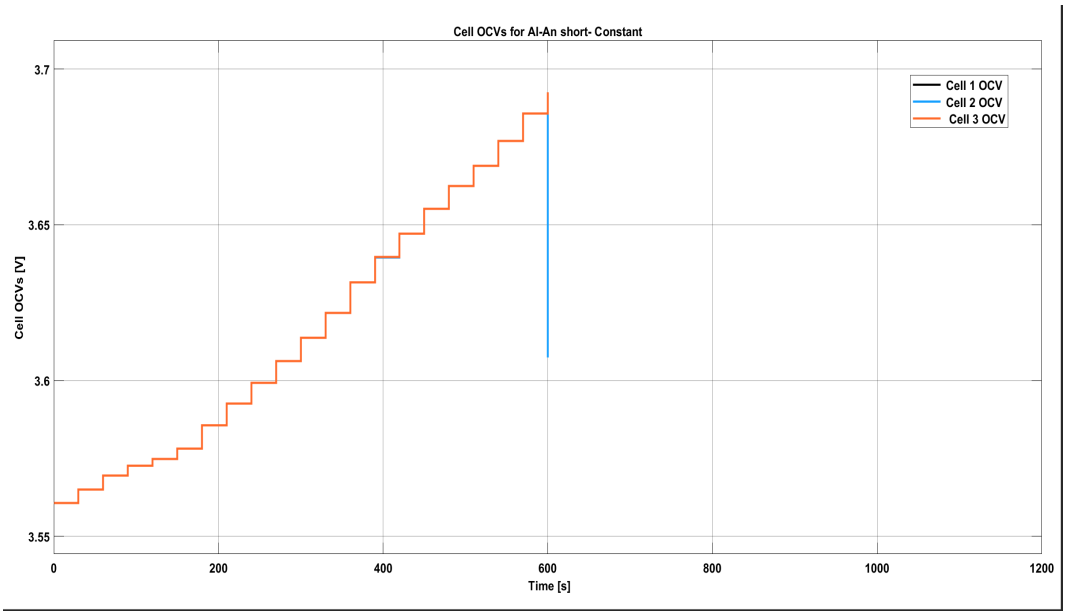

Figure 4.27: Cell OCVs obtained for Al-An short after co-simulation

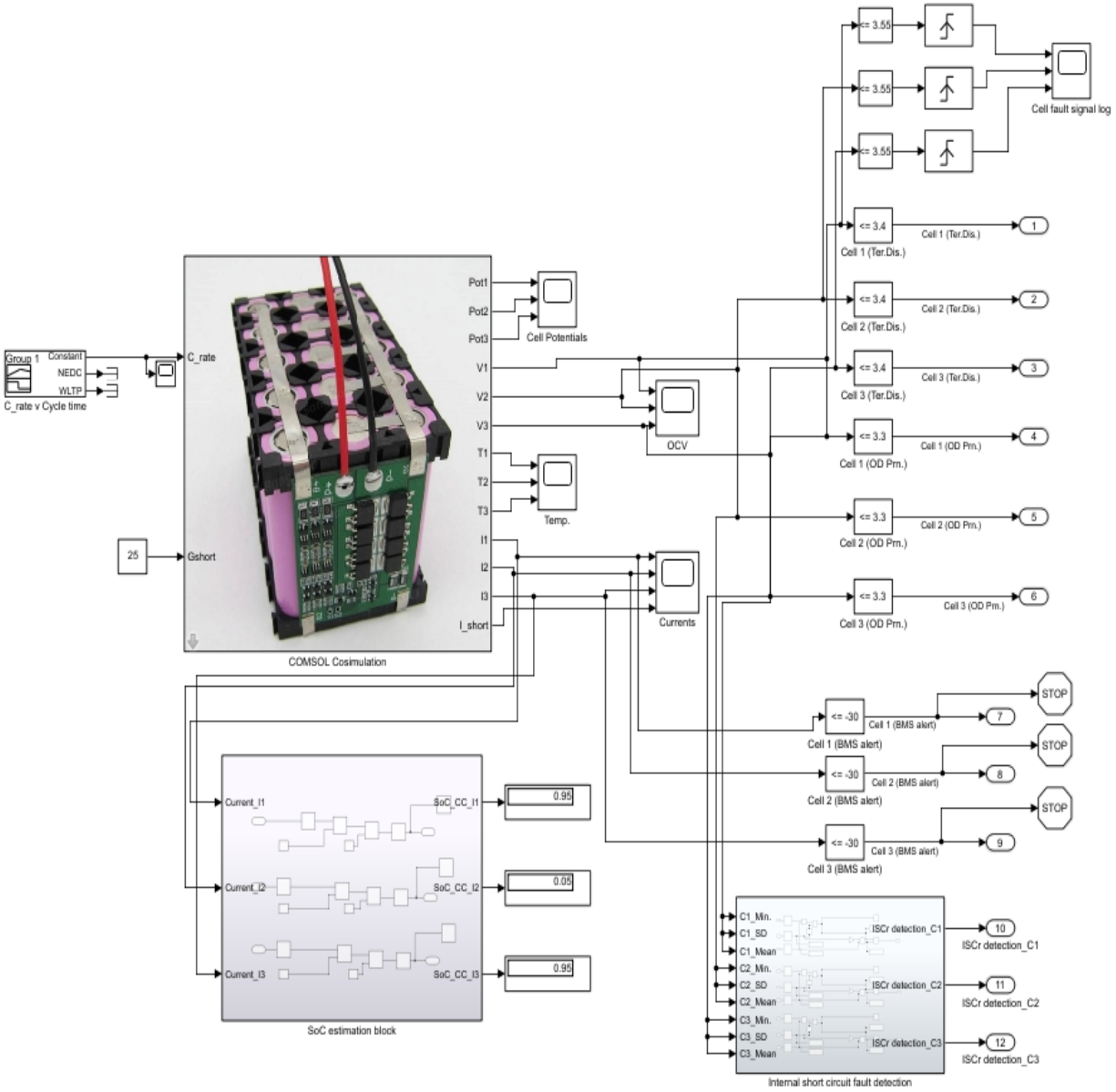

Figure 4.28: FMU for co-simulation of Al-An short

The high short circuit conductance for Al-An case results in a rapid decrease in second cell's OCV. This leads to a high short circuit current and which triggers the current limit set for alerting the BMS. This stops the simulation as the limit is surpassed as evident in Fig.4.27. The FMU model with constant C-rate as the drive cycle input along with 25S as the short circuit conductance value are considered for this case.

Cu-Ca short

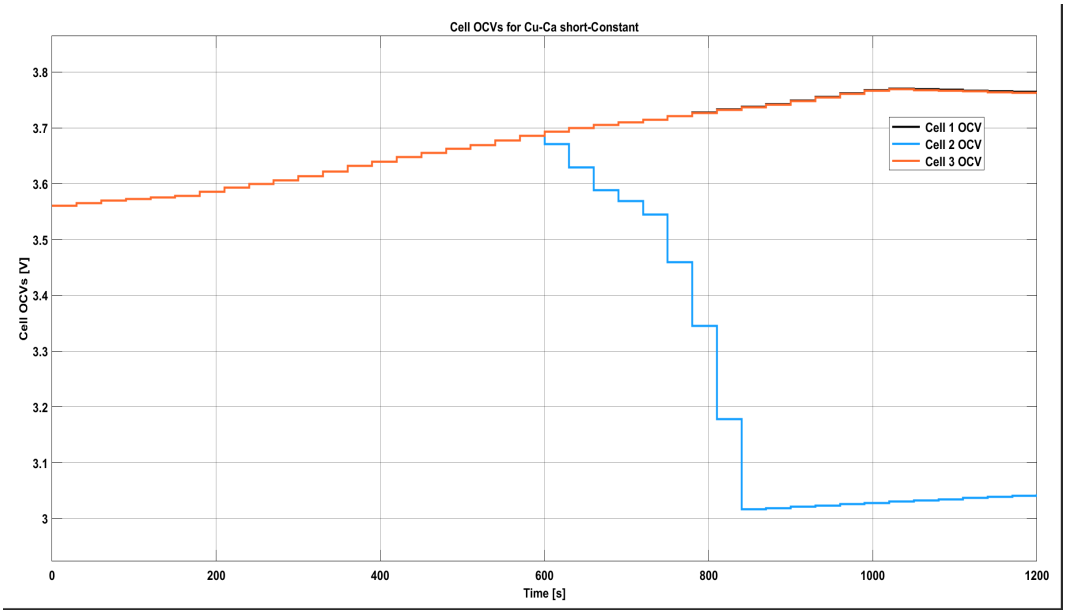

Figure 4.29: Cell OCVs obtained for Cu-Ca short after co-simulation

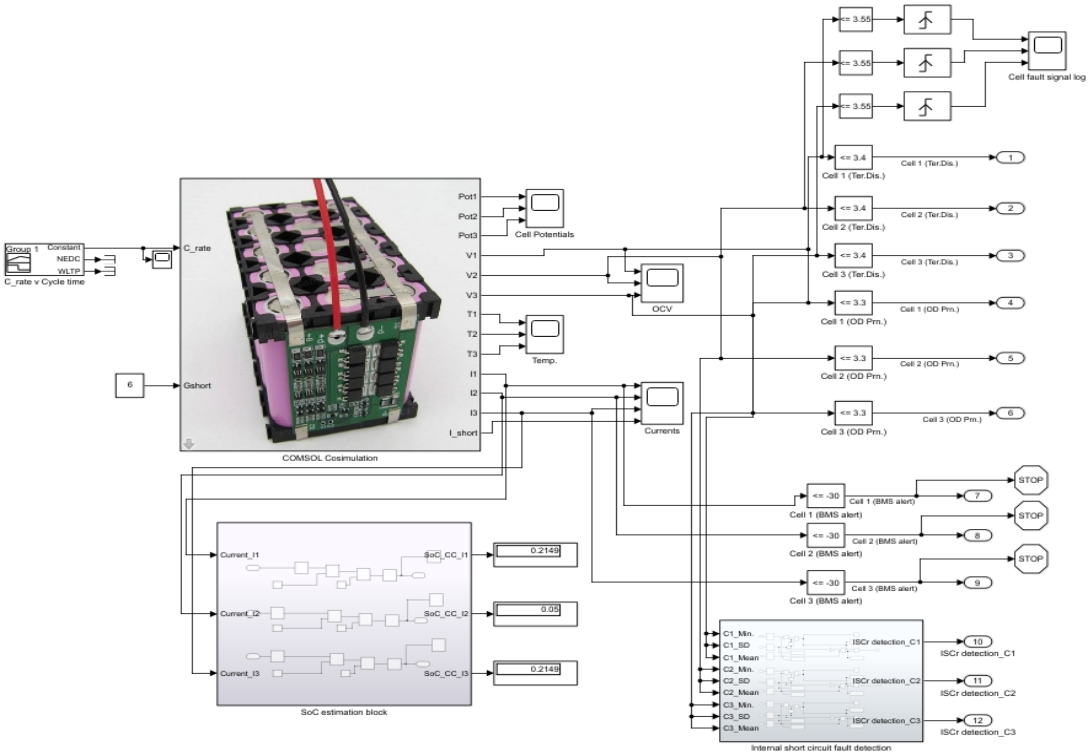

Figure 4.30: FMU for co-simulation of Cu-Ca short

A lower short circuit conductance for the Cu-Ca case is considered. The second cell's OCV falls but a slower rate than Al-An short. This results in a lower SC current. The current limit for alerting the BMS is not triggered as evident in Fig.4.29 and the simulation is not stopped. FMU model with constant C-rate as drive cycle input along with 6S as the short circuit conductance value are considered for this case.

Fault Detection for drive cycle with constant C-rate

Al-An short

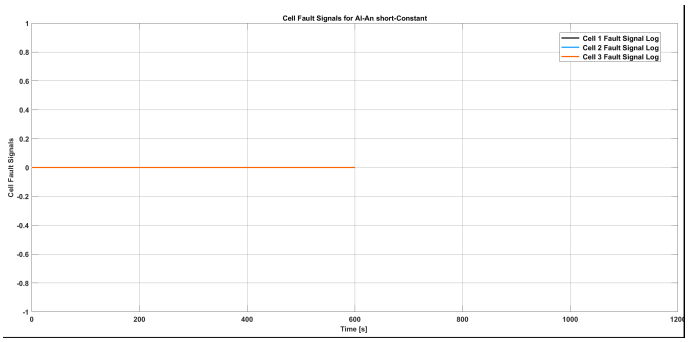

Figure 4.31: Cell fault detection time for Al-An short

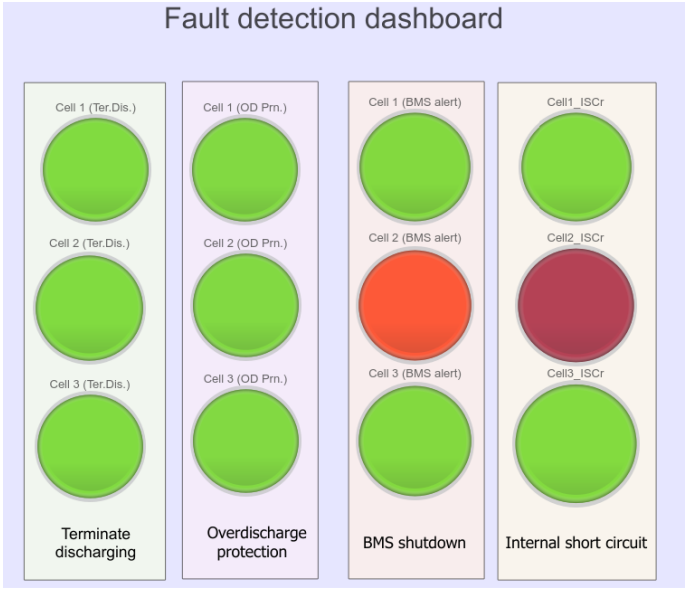

Figure 4.32: Fault detection dashboard for Al-An short

The high short circuit conductance for the Al-An case results in higher current. This makes the rapid increase of the temperature possible increasing the chances of thermal runaway making it all the more important for the fault to be detected faster. The current limit for BMS alert is triggered as evident from Fig.4.31 which acts quickly before other signals are triggered. Once the signal is triggered an internal short circuit in cell 2 is detected. The quick fault detection fault is shown

in Fig.4.32. The fault signal log stops at 600s once second cell's fault is triggered. The fault signal not visible since the simulation is stopped before logging the signal.

Cu-Ca short

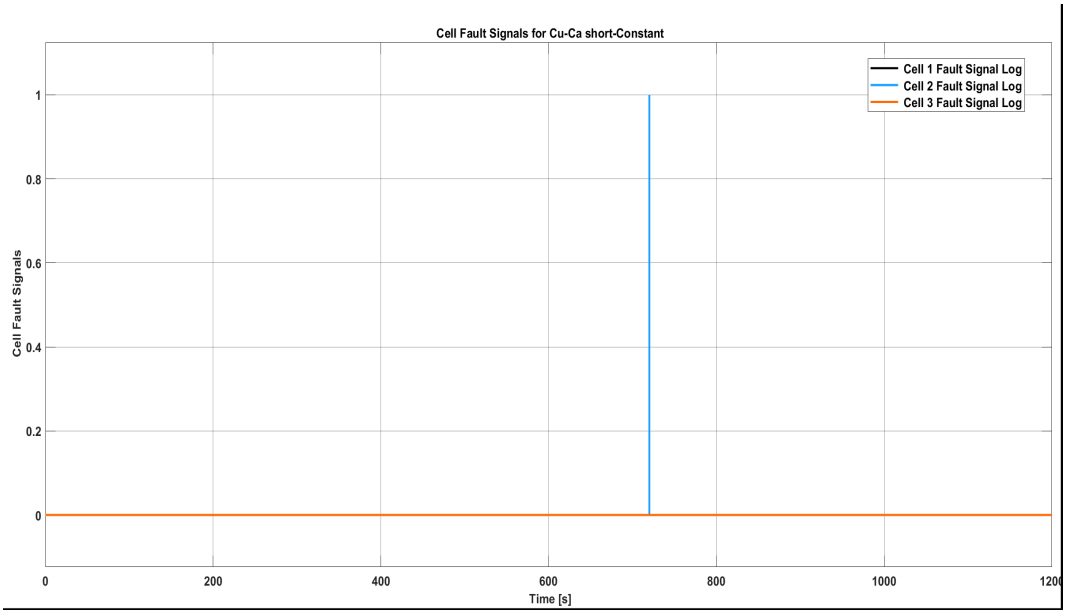

Figure 4.33: Cell fault detection time for Cu-Ca short

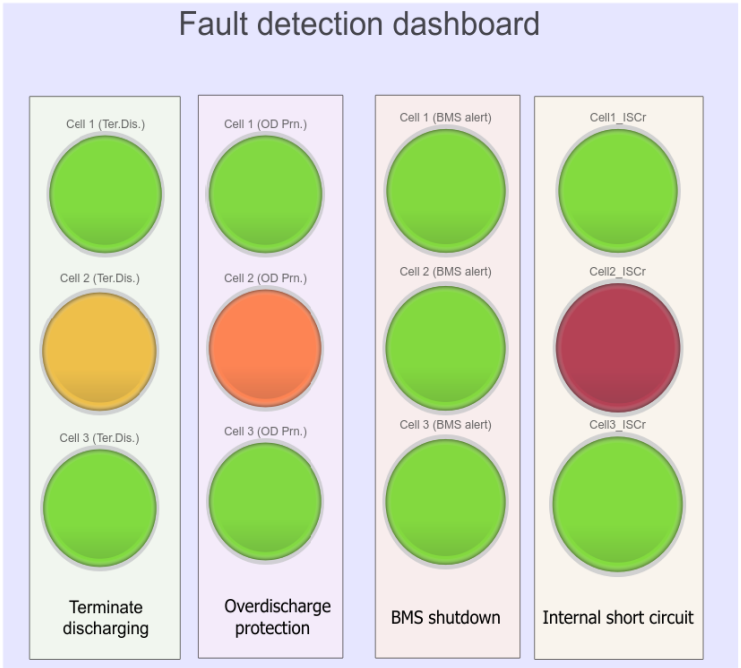

Figure 4.34: Fault detection dashboard for Cu-Ca short

In this case, there is a lower short circuit conductance compared to the Al-An case. This results in lower current and temperature. The current limit for BMS alert is not triggered. However, the fault signals for 'Terminate Discharge' and 'Overdischarge protection' are triggered after which the internal short circuit in cell 2 is detected. The fault is detected at 680s after which the fault signal log (shown in blue for cell 2 in Fig.4.33) stops.

4.2 Fault Detection with WLTP Driving Cycle

4.2.1 Electric Vehicle Simulation (WLTP)

The simulation of the vehicle model yields the following results:

1. Battery Power vs Vehicle Speed for WLTP Drive Cycle

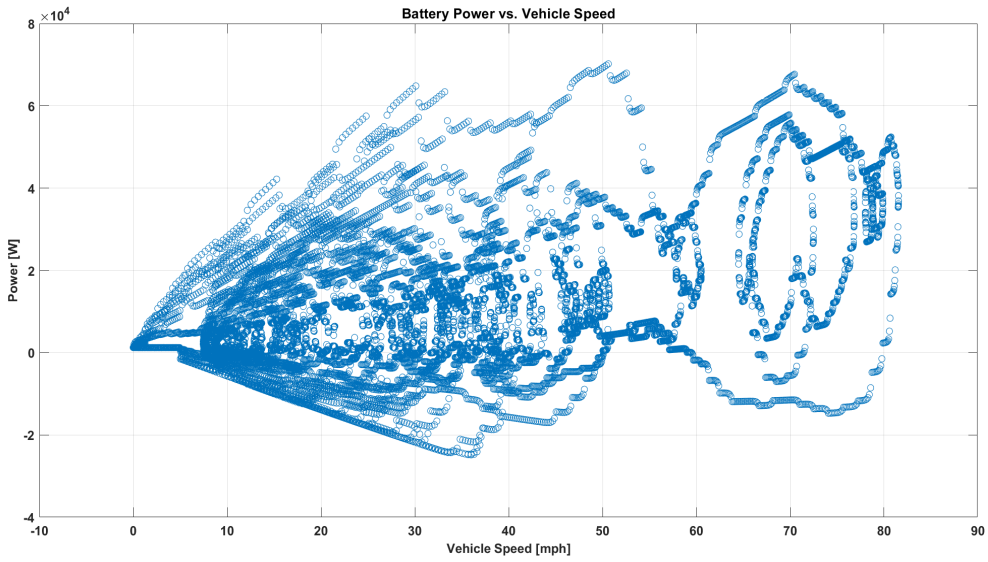

Figure 4.35: Battery Power vs Vehicle Speed for WLTP Drive Cycle

The plot shown in Fig.4.35 enunciates that the battery power drawn is in accordance to demands of the WLTP drive cycle. In the low speed region, the power demand is low and more frequent. In the high speed region, the power demand is higher and less frequent as is usual case in day-to-day scenario.

2. Battery Current vs Time for WLTP Drive Cycle

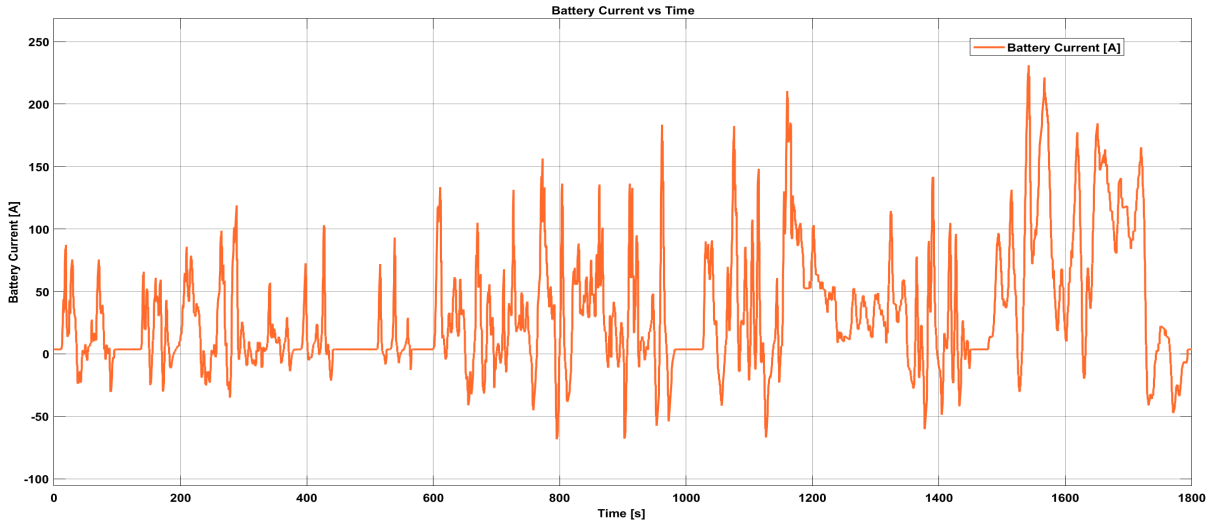

Figure 4.36: Battery Current vs Time for WLTP Drive Cycle

Fig.4.36 shows the battery current following the same path of WLTP and reflects the demands of the drive cycle. In the higher demand region, motor demand increases and the battery current increases. In the lower demand region, the motor demand decreases and the battery current decreases.

3. Motor Power vs Battery Power for WLTP Drive Cycle

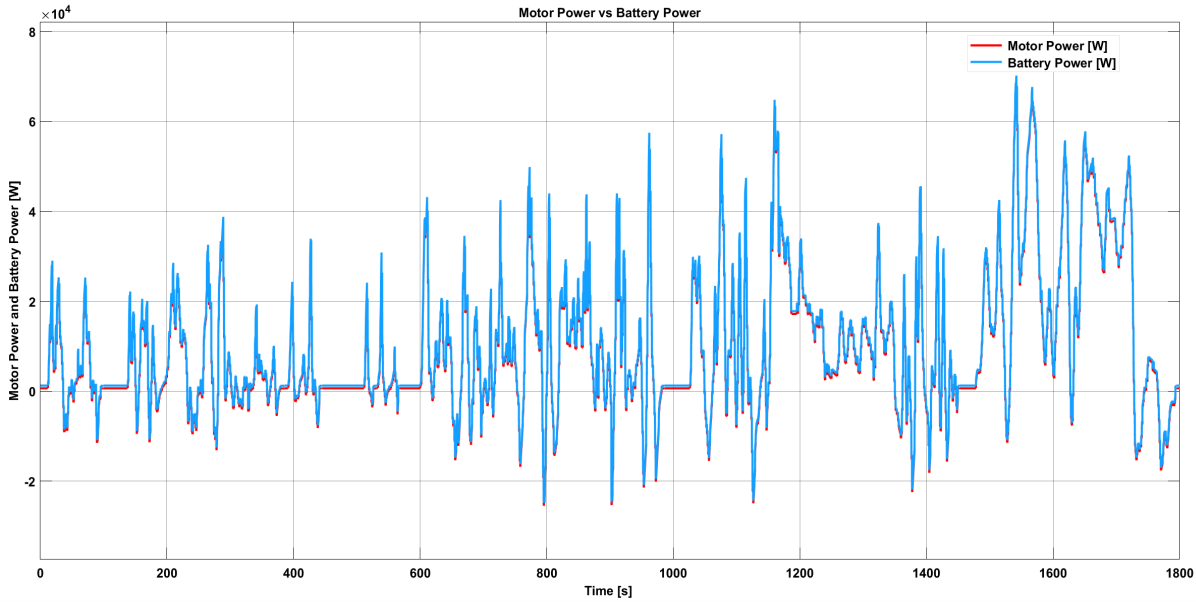

Figure 4.37: Motor Power and Battery Power vs Time for WLTP Drive Cycle

Battery power follows motor power closely and is in accordance with the demands of the vehicle. In the low speed region, the power demand is low. In the high speed region, the power demand is higher.

4. Cell C-Rate for WLTP Drive Cycle

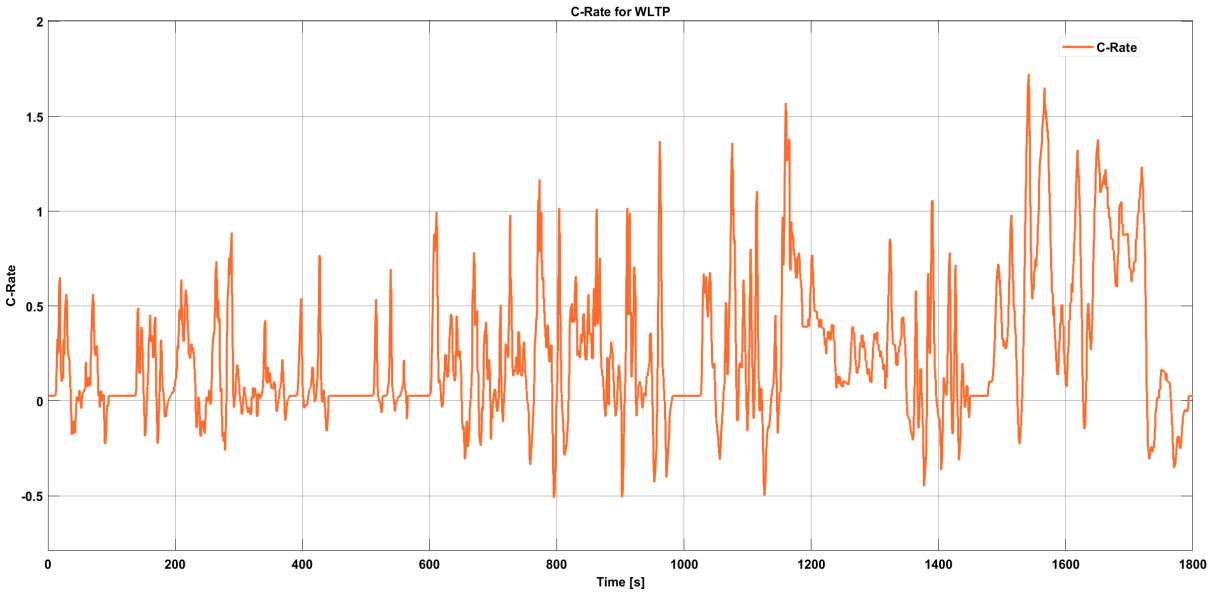

Figure 4.38: Cell C-Rate for WLTP Drive Cycle

The battery C-rate follows the same path as the battery current. Higher the demand, the motor demand increases. This leads to an increase in battery current resulting in a higher C-rate. Lower the demand, the motor demand decreases. Then, the battery current decreases which effects a lower C-rate.

4.2.2 Internal Short Circuit Detection with COMSOL Simulation (WLTP)

Al-An short

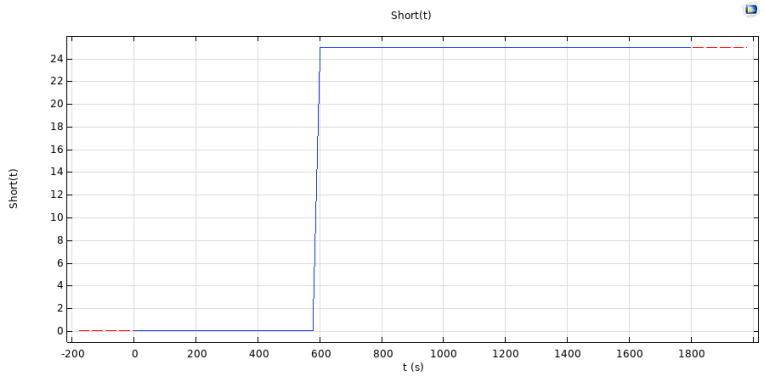

Figure 4.39: Al-An internal short circuit trigger cycle

The short circuit trigger cycle shown in Fig.4.39 activates the Al An internal short which has a conductance of 25 S at 600s till the end of the drive cycle at 1800s.

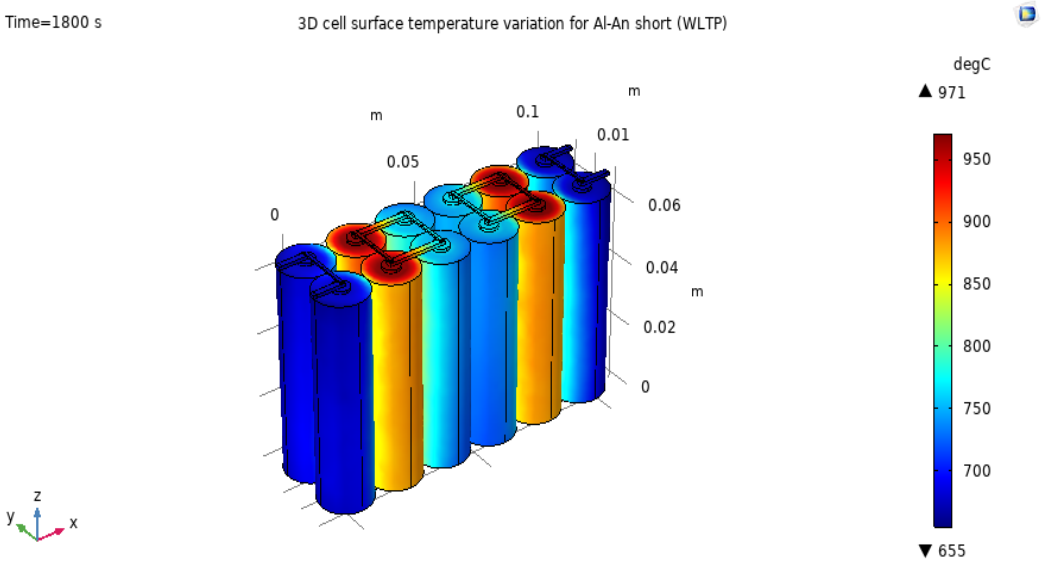

Figure 4.40: 3D cell surface temperature variation for Al-An short

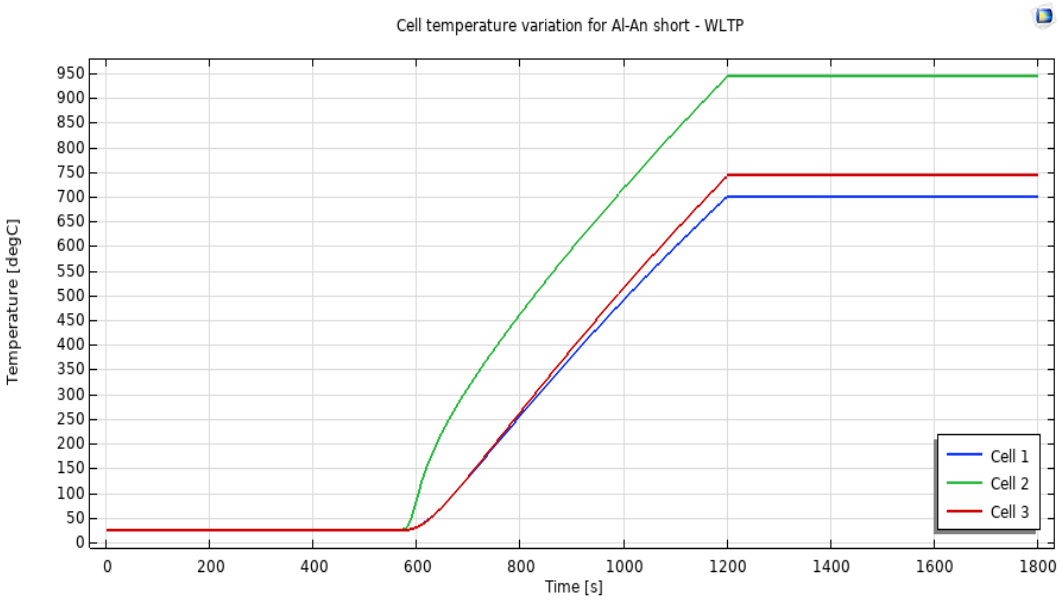

Figure 4.41: 1D Cell temperature variation for Al-An short

From Fig.4.40, we can observe that the surface temperature distribution rises to a maximum temperature of 971°C at the internally shorted second cell while the first cell remains at a relatively lower temperature. 1D temperature distribution over the cells as in Fig.4.41 indicates the severity of the Al-An internal short circuit fault. After 600s, a gradual increase in temperature is observed. This results in a high power short owing to the low electrical resistivity offered by the anode.

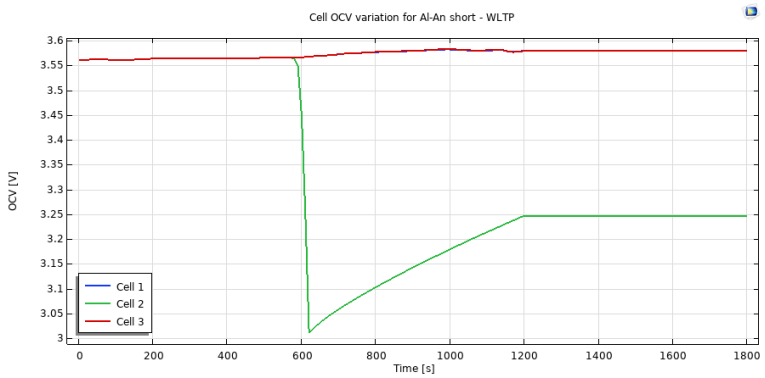

Figure 4.42: Cell OCV variation for Al-An short

The cell OCVs as shown in Fig.4.42 are dependent on the cell SoC and the temperature. As soon as the fault is triggered, the OCV of Cell 2 falls at a sharp rate and is accompanied with a high short circuit current. After certain time, it seems to stabilize which could be attributed to a possible flow of current in the opposite direction.

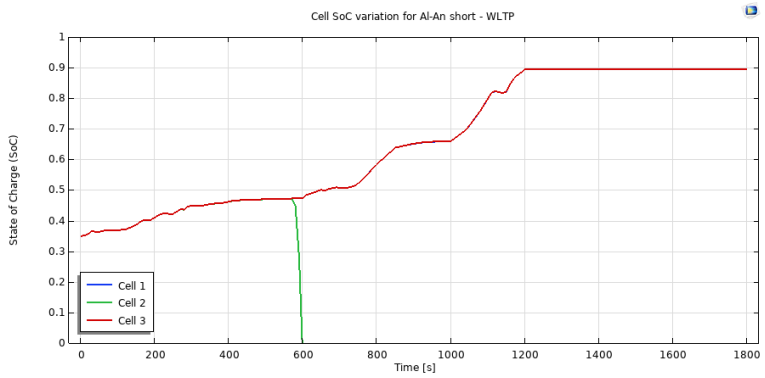

Figure 4.43: Cell SoC variation for Al-An short

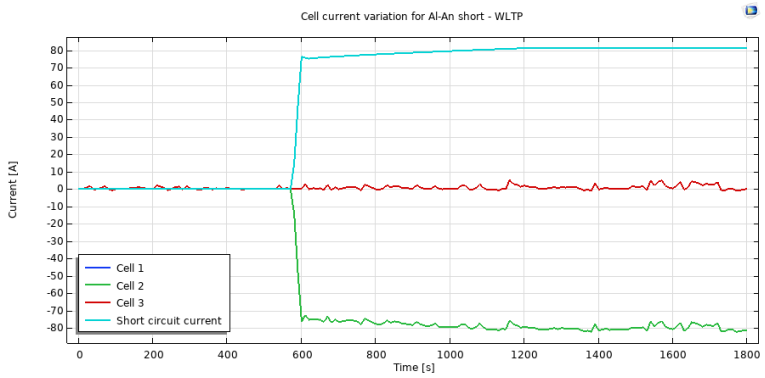

Figure 4.44: Cell current variation for Al-An short

The SoC of cell 2 as indicated in Fig.4.43 falls suddenly once the fault is triggered at 600s and the SoCs of the other cells increase. This is due to the rapid increase in discharge current. Referring Fig.4.44, we notice that the short circuit fault current reaches close to 85 A rendering cell 2 unstable in a very short span of time. This ISC scenario has high thermal activity due to the anode's low very low electrical resistivity.

Cu-Ca short

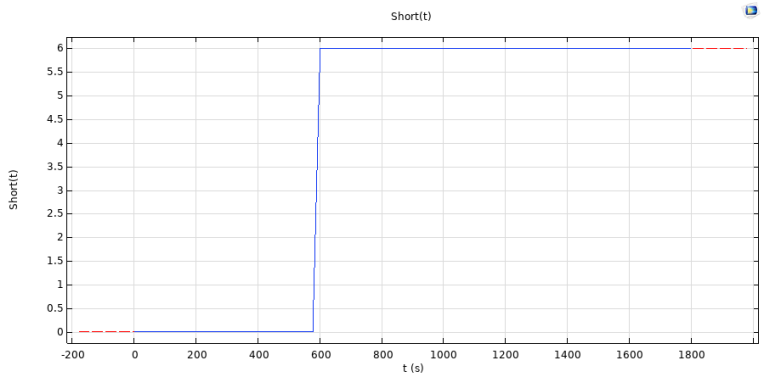

Figure 4.45: Cu-Ca internal short circuit trigger cycle

The short circuit trigger cycle in Fig.4.45 activates the Cu-Ca internal short which has a conductance of 6S at 600s till the end of the drive cycle at 1800s, which is the least among all 4 cases of internal short circuit scenarios.

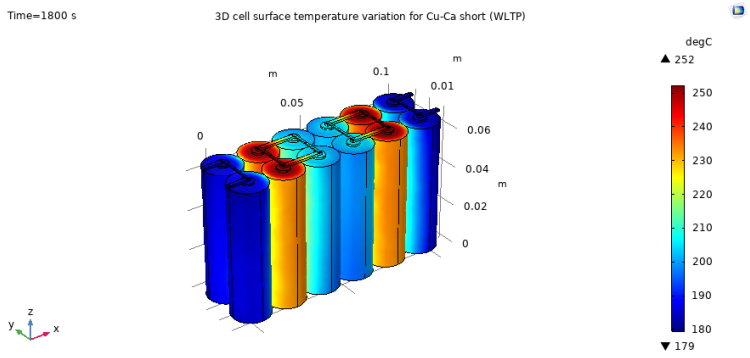

Figure 4.46: 3D cell surface temperature variation for Cu-Ca short

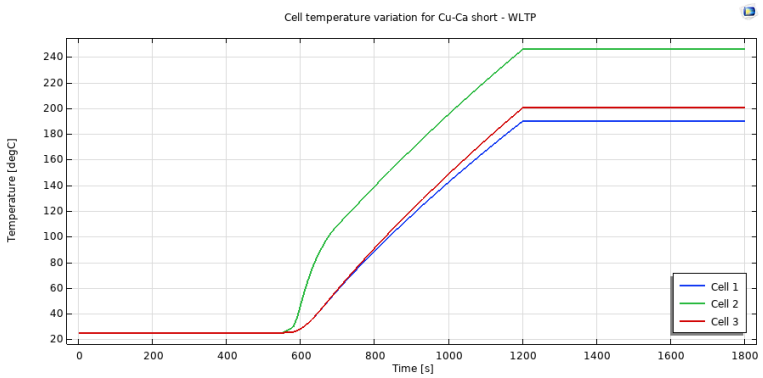

Figure 4.47: 1D Cell temperature variation for Cu-Ca short

The effect of the Cu-Ca internal short in Fig.4.46 indicates that temperature of second cell increases rapidly to a maximum of 252°C. The reason for the lower temperature rise is because the cathode material is a poor conductor of heat and consequently the heat released is not enough to trigger any further chemical reactions. This is reinforced by Fig.4.47 which exhibits the 1D temperature distribution plot.

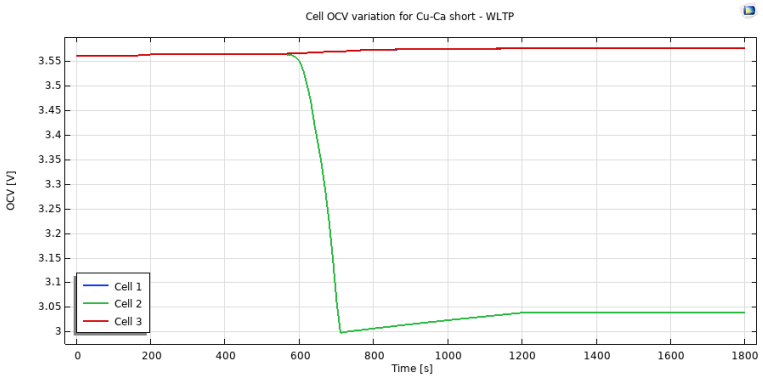

Figure 4.48: Cell OCV variation for Cu-Ca short

The OCVs of cells 1 and 3 as indicated in Fig.4.48 rise to a certain value around 3.55 V and stabilizes as the drive cycle input becomes zero This is 0.2V lower compared to the same case with constant C rate Cell 2 OCV falls as soon as the fault is triggered but at a much slower rate as compared to the Al-An short because of the low short circuit conductance values.

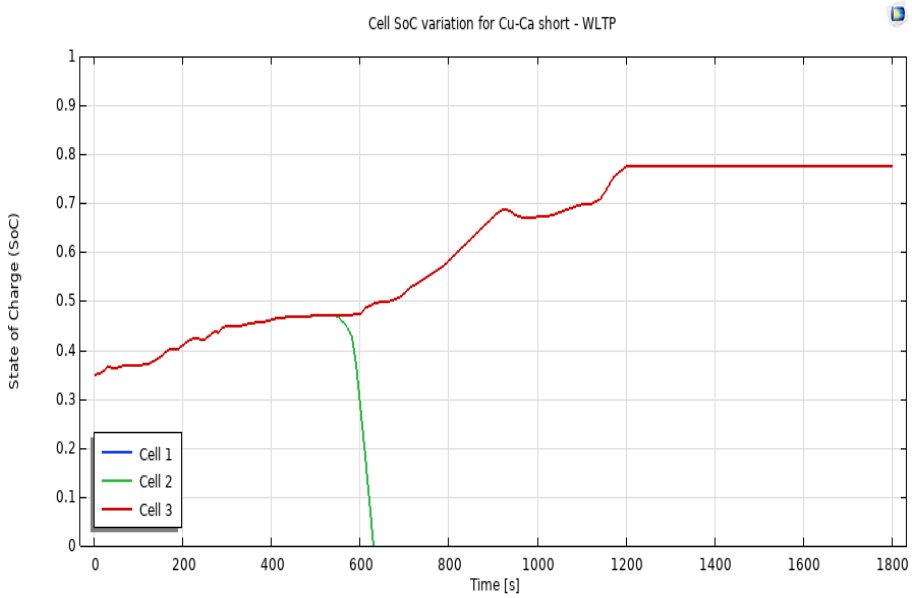

Figure 4.49: Cell SoC variation for Cu-Ca short

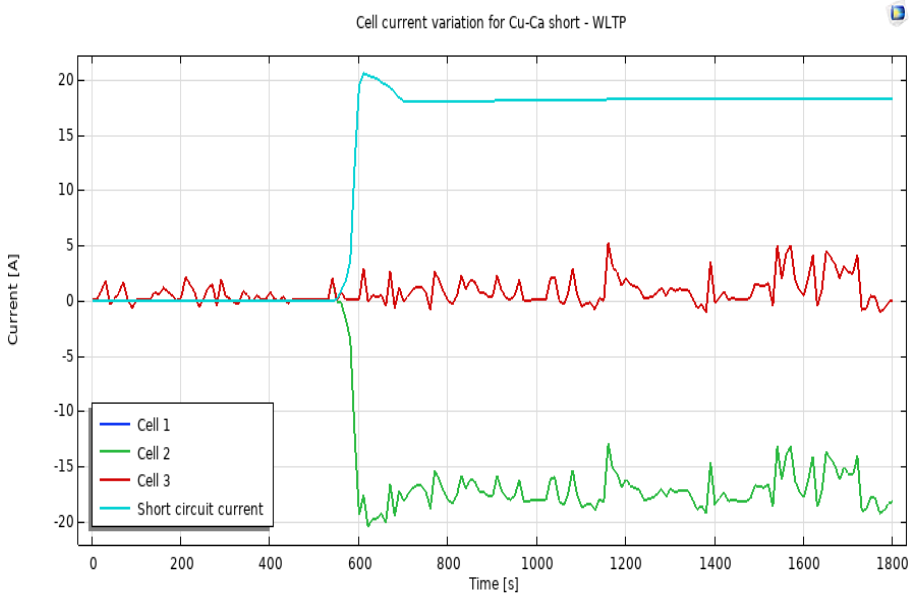

Figure 4.50: Cell current variation for Cu-Ca short

The SoC falls at a slightly slower rate than the previous type of internal short circuit fault due to the increase in discharge current and is expressed in Fig.4.49. The cell short circuit current shown in Fig.4.50 is quite low as compared to all other cases, with magnitudes of around 20 A.

Cu-Al short

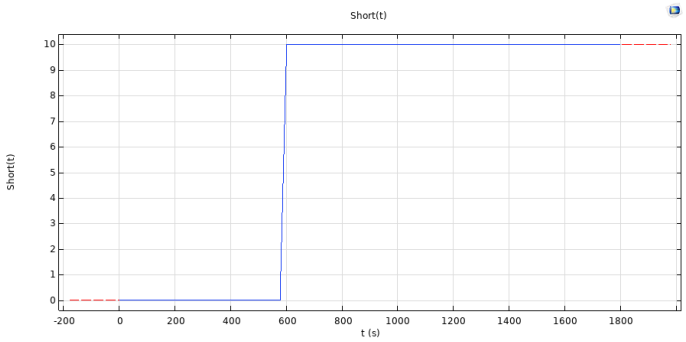

Figure 4.51: Cu-Al internal short circuit trigger cycle

The short circuit trigger cycle in Fig.4.51 activates the Cu-Al internal short which has a conductance of 10 S at 600 s till the end of the drive cycle at 1800 s.

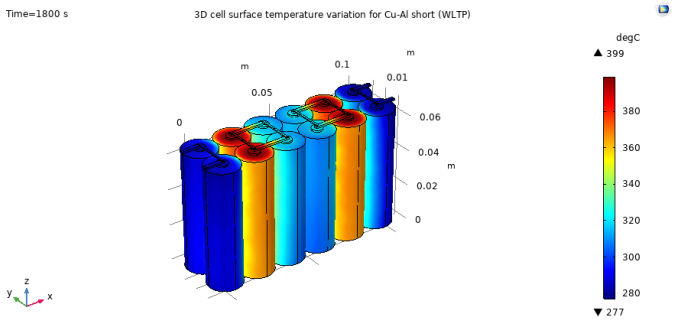

Figure 4.52: 3D cell surface temperature variation for Cu-Al short

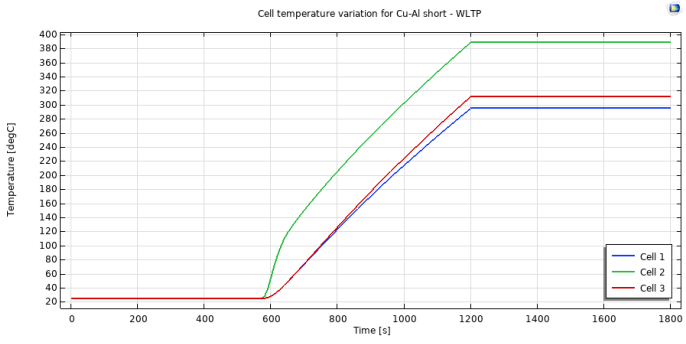

Figure 4.53: 1D Cell temperature variation for Cu-Al short

In this case the temperature rises to about 400°C and is exhibited in Fig.4.52 and Fig.4.53. This case is similar to the cell's terminals being externally connected with a low resistance path. The same case for the drive cycle with a constant C-rate

had a surface temperature about 10°C higher. Though the temperature rises to a high value, the materials are good conductors of heat and hence can dissipate heat quickly and pose a comparatively lesser threat than the other cases.

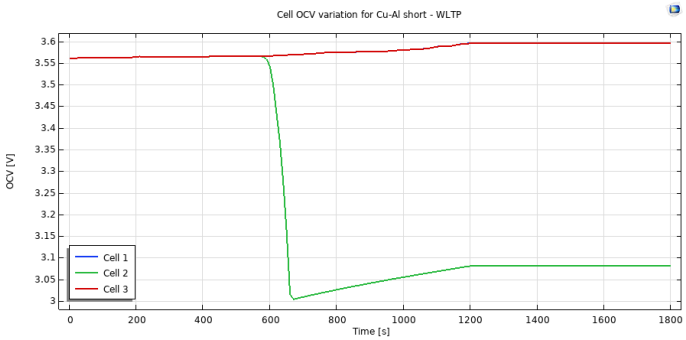

Figure 4.54: Cell OCV variation for Cu-Al short

The OCVs of cells 1 and 3 as indicated in Fig.4.54 rise to a certain value and stabilize as the drive cycle input becomes zero. The second cell's OCV falls as soon as the fault is triggered at a quicker rate due to the larger short circuit conductance value.

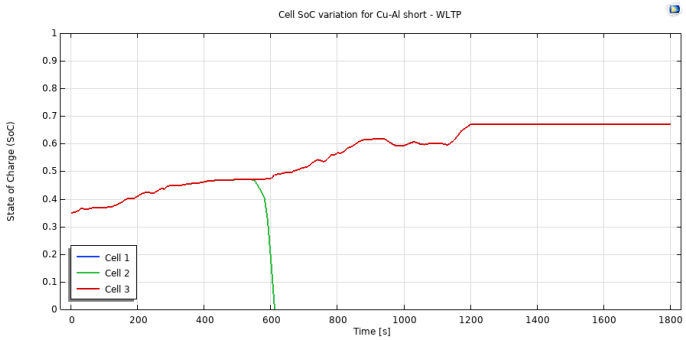

Figure 4.55: Cell SoC variation for Cu-Al short

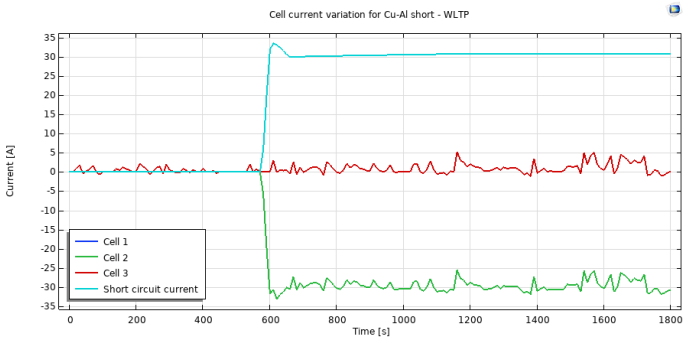

Figure 4.56: Cell current variation for Cu-Al short

The state of charge variations for each cell as in Fig.4.55 are much steeper for this

case as the short circuit current increases and due to the rapid fall of OCV. The SoC falls faster than the Cu-Al case but is slower than the Al An case. From Fig.4.56, the second cell's short circuit current is around 35 A, but the temperature rise accompanying the current rise can lead to a thermal runaway scenario. A small increase in currents of cells 2 and 3 can also be observed.

An-Ca short

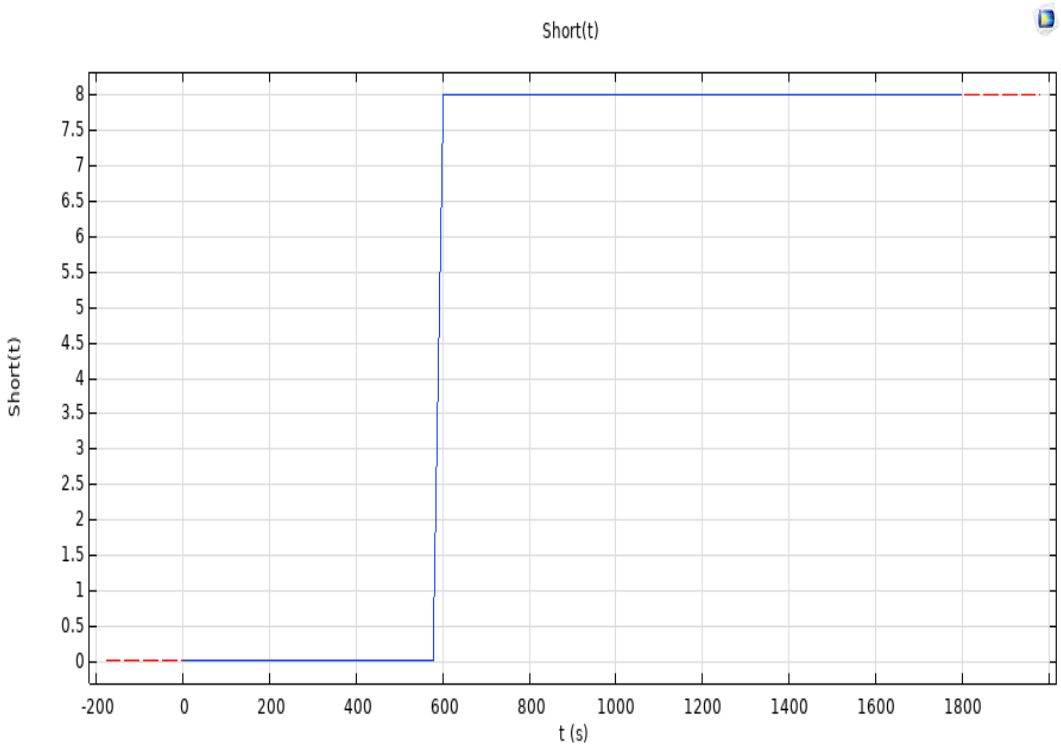

Figure 4.57: An-Ca internal short circuit trigger cycle

Short circuit trigger cycle shown in Fig.4.57 is activated to simulate the An Ca internal short which has a conductance of 8S at 600s till the end of the drive cycle at 1800s.

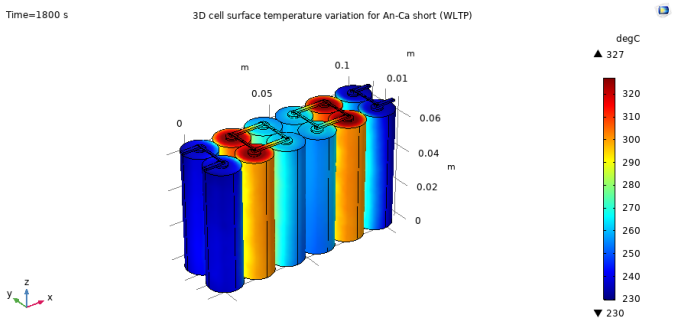

Figure 4.58: 3D cell surface temperature variation for An-Ca short

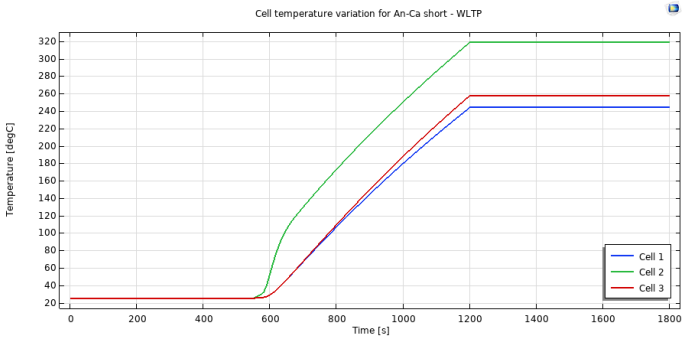

Figure 4.59: 1D Cell temperature variation for An-Ca short

Referring Fig.4.58, the temperature rises to about 327°C which is an important figure as the An-Ca short is the most probable type of fault observed in Li ion cells. The gradual temperature rise as seen in Fig.4.59 is in between the 25S and the 6S case. This is due to the cathode's low material conductivity and hence higher resistance or lower conductance.

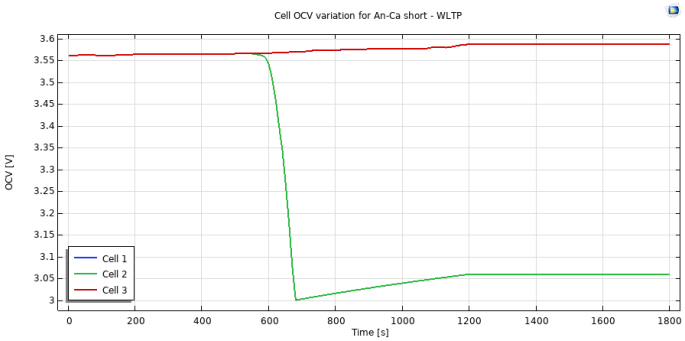

Figure 4.60: Cell OCV variation for An-Ca short

The OCVs of cells 1 and 3 as indicated in Fig.4.60 rise to a certain value and stabilize as the drive cycle input becomes zero. Second cell's OCV falls as soon as the fault

is triggered but at a slower rate compared to the 10S internal short circuit case but faster than the 6S internal short circuit case.

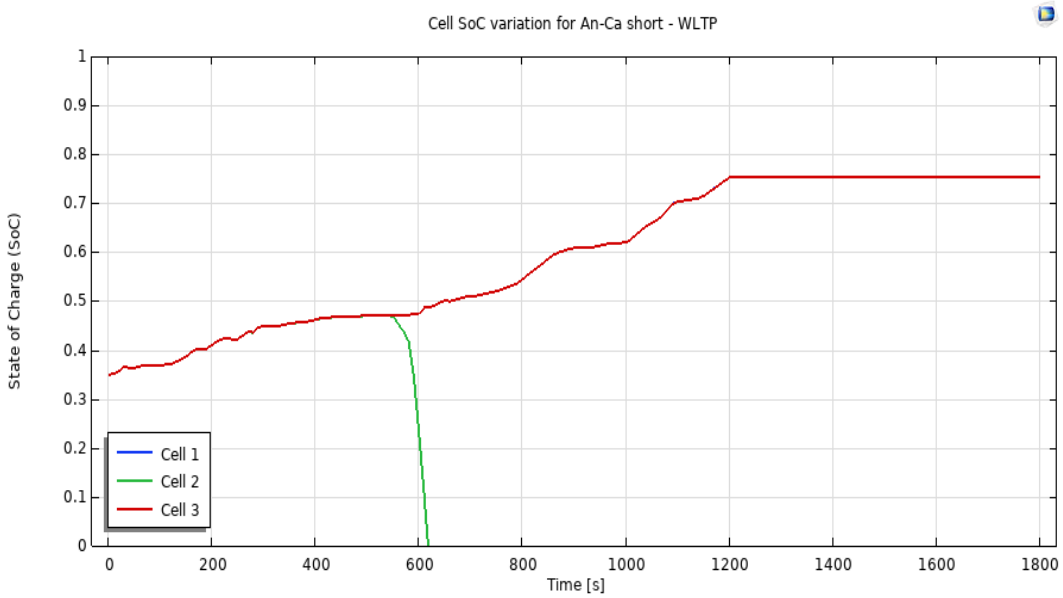

Figure 4.61: Cell SoC variation for An-Ca short

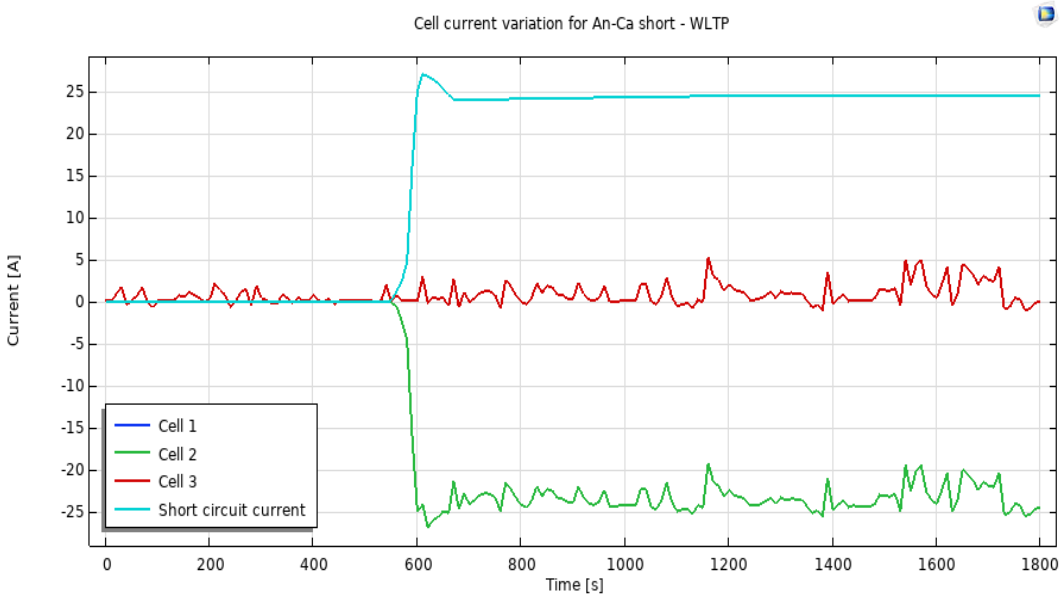

Figure 4.62: Cell current variation for An-Ca short

The state of charge variations for each cell as in Fig.4.61 are much slower than the 10S case and is reflected in the rise of the short circuit current and fall of OCV. The cell short circuit current seen in Fig4.62 is around 30 A, since this is a higher resistance or lower conductance short than the 10S internal short circuit case.

4.2.3 Internal Short Circuit Detection with Co-simulation (WLTP)

Al-An short

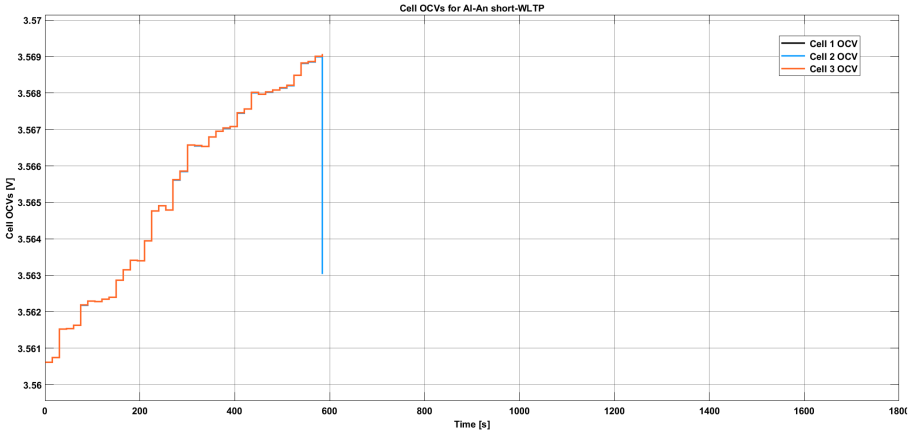

Figure 4.63: Cell OCVs obtained for Al-An short after co-simulation

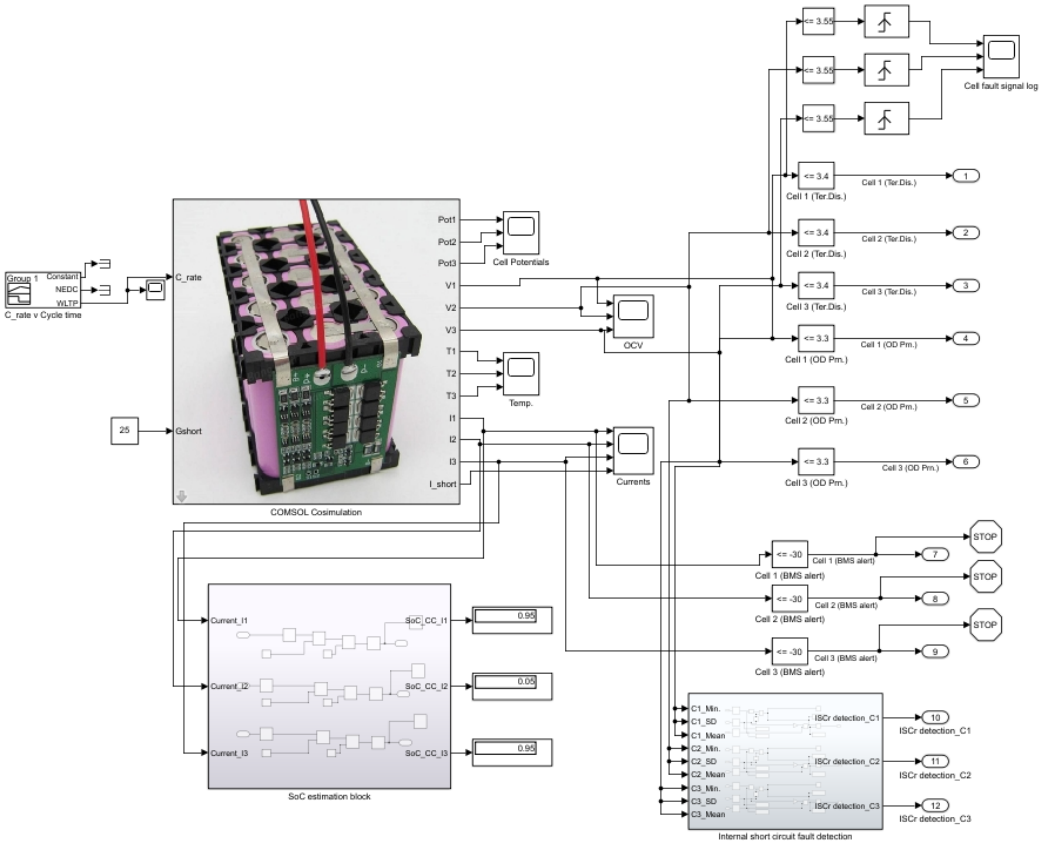

Figure 4.64: FMU for co-simulation of Al-An short

The high short circuit conductance for Al-An short circuit case results in the decrease in second cell's OCV. The high SC current triggers the current limit and alerts the BMS. The simulation is stopped the moment the limit is exceeded as shown in Fig.4.63. OCV falls to a lower voltage than the value observed for the previous case with the drive cycle with a constant C-rate. An FMU model with WLTP as drive cycle input along with 25S as the short circuit conductance value is considered for this case.

Cu-Ca short

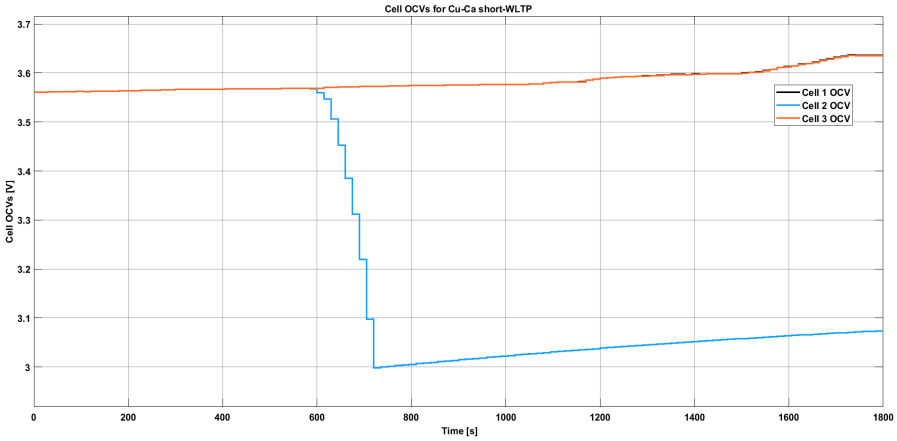

Figure 4.65: Cell OCVs obtained for Cu-Ca short after co-simulation

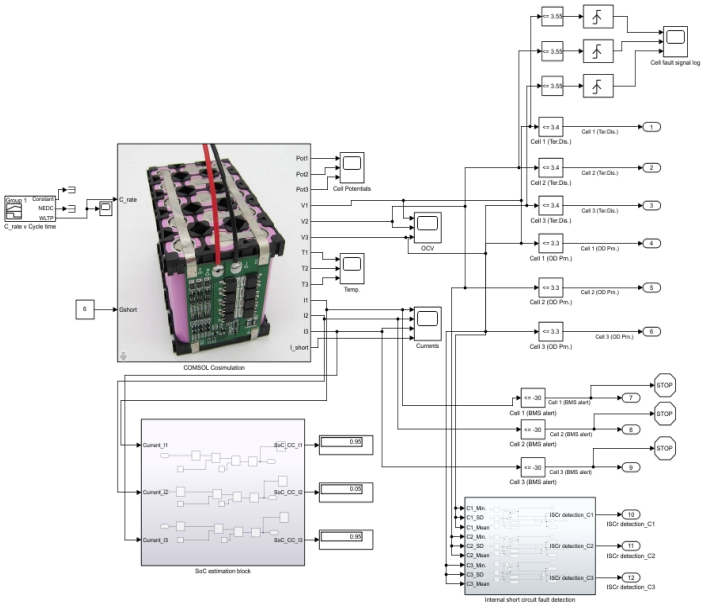

Figure 4.66: FMU for co-simulation of Cu-Ca short

A lower short circuit conductance for the Cu-Ca case results in the second cell's OCV decreasing but a rate slower than Al-An case. Since this brings about a lower short circuit current, the current limit for BMS alert is not triggered as evidenced in Fig.4.65. Thus, the simulation is not stopped and the OCV falls slightly faster for WLTP compared to the previous case. An FMU model with WLTP as drive cycle input along with 6S as the short circuit conductance value is considered for this case.

Fault Detection for WLTP

Al-An short

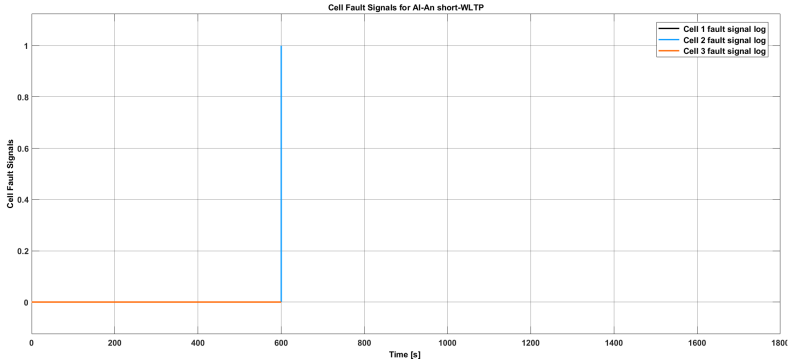

Figure 4.67: Fault detection dashboard for Al-An short

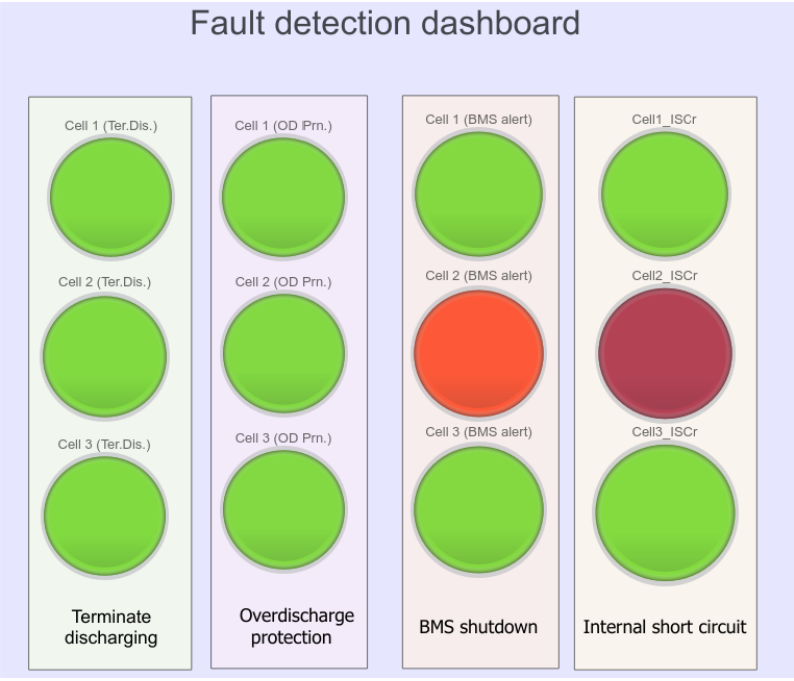

Figure 4.68: Fault detection dashboard for Al-An short

As mentioned earlier, a high short circuit conductance for Al-An case results in a higher current and temperature. This results in a higher probability of thermal runaway which makes it all the more important for this fault to be detected faster. The current limit for BMS alert triggered after which the system acts quickly before other signals are triggered. From Fig.4.68, the internal short circuit in the second cell is detected. The fault is detected quickly during which time the fault signal log stops at 600s as a result of the fault from second cell.

Cu-Ca short

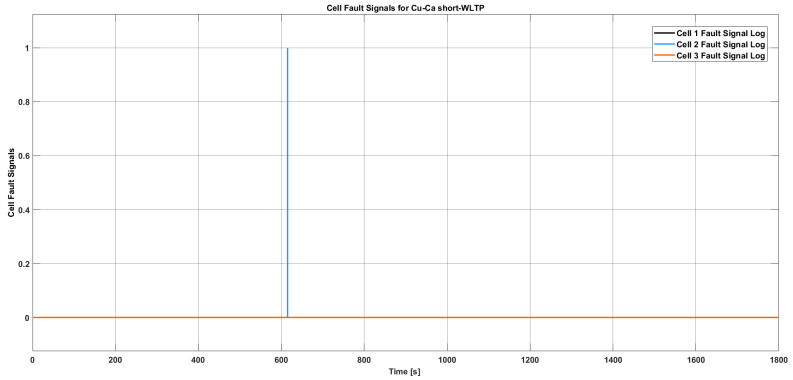

Figure 4.69: Fault detection dashboard for Cu-Ca short

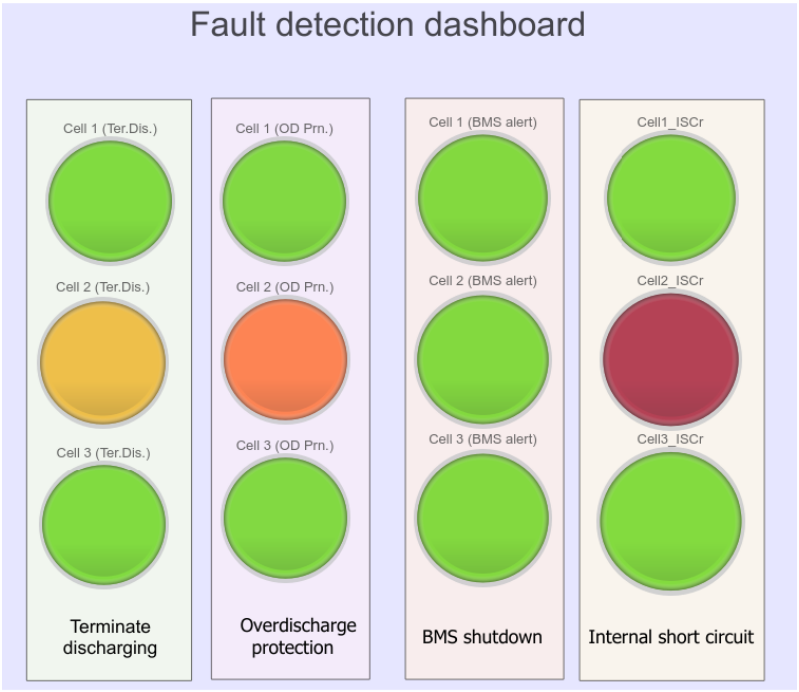

Figure 4.70: Fault detection dashboard for Cu-Ca short

A lower short circuit conductance than the Al-An case results in a lower current and temperature. The current limit for BMS alert is not triggered as a result and is evident from Fig.4.69. The fault signals for 'Terminate Discharge' and 'Overdischarge protection' are triggered when the internal short circuit in the second cell is detected. Once the fault is detected at 620s, the fault signal log stops.

4.3 Reconfigurable Battery Systems

Existing battery management systems mainly focus on state monitoring and control of battery systems packed in fixed configurations. Allowing dynamic reconfiguration of battery cells allows individual and flexible manipulation of cells. Such systems known as Reconfigurable Battery Systems (RBS) are a visible research area with multiple real-world benefits, especially for the growing hybrid and electric vehicle markets.

Internal short circuits cause cell damage which spread to neighbouring cells and destroys the entire system. This leads to energy and resource wastage and further reaction with other cell materials possibly causing thermal runaway. This scenario can be avoided by RBS which quickly disconnect the faulty cells while reconnecting the remaining normal ones. Local faults can be isolated so that other cells can keep working normally without significantly affecting the system level functionalities and resulting in increased performance and upgraded fault tolerance. Charge imbalance largely reduces the available charge capacity of cells resulting in under-utilization of some cells and over-utilization of other cells, resulting in undesirable conditions such as overcharging, overdischarging, internal short circuit and thermal imbalance. Available research suggests that RBS needs about half of the time as conventional systems to reach the state of charge equalization with no additional cell balancing circuitry.

RBSs help schedule the operation of batteries for faster and enhanced energy conversion during both charging and discharging. RBS can also be used for coordinating batteries of different age and chemistry. With second life of batteries becoming increasingly relevant to maintain a sustainable product life-cycle, RBSs can be used for their increased balancing capability resulting in their use in stationary energy storage applications.

In order to isolate the faults, different switch operations may be performed, depending on the circuit designs. When battery cells are in parallel, it is easy to skip a cell by using only one switch. If the cell to be isolated lies in a series connected cell string, at least two switch operations need to be conducted simultaneously. Thus, care must be taken to coordinate multiple switch operations so that no open and short circuits are incurred.

MOSFETs of low cost, high conduction efficiency, good performance are used in RBS increasing forward reverse current control. Customized terminal voltage, current,

and power can be implemented using RBSs while avoiding inverters and converters used for conventional battery systems.

A growing amount of research focuses on developing controllable, repeatable fault substitute tests and high fidelity models for simulating real faults. This is especially useful for the internal short circuits where RBS-based fault tolerant controllers could be used for rapid and efficient fault handling [31].

5
Conclusions & Future work

5.1 Conclusions

In this thesis, the various faults that occur in a Lithium ion cell have been explained and the most common type of fault, the internal short circuit has been studied. A method to detect internal short circuits has been implemented for different scenarios of the same. For simulation, a Battery Electric Vehicle (BEV) model was used to obtain the cell C-rate which was later used as an input to the COMSOL cell model. Through this step, an understanding of the demands on the battery pack inside an electric vehicle was developed.

A resulting Functional Mockup Unit (FMU) from the COMSOL model was further utilized to develop an internal short circuit detection method based on the cell OCVs. This model was used to co-simulate it for a drive cycle with constant C-rate and the WLTP drive cycle. The constant C-rate drive cycle was used to test whether the model functioned properly and was observed to give correct results. The WLTP drive cycle was utilized to simulate a real-case scenario and test the demands of a battery pack. It was observed that the Aluminium-Anode short circuit case was the most dangerous and could potentially lead the battery into thermal runaway. It was also observed that lower the short circuit resistance, higher was the short circuit current and temperature.

The communication step used during co-simulation played an important role in determining the speed of simulation. The lesser the communication step, the more detailed were the results and longer was the simulation time. Using conservative voltage limits to avoid overdischarge of non-faulted cells was observed to give satisfactory results.

5.2 Future work

Improvements could be made to include a more detailed COMSOL model of the battery pack to reflect the interior structure of a cell. This can increase the result accuracy and areas in the cell can be localized and studied in depth.

Other materials which are increasingly used in upcoming battery chemistries like Silicon, Lithium metal or Air, could be explored and results could be organized for different cell chemistries keeping in mind their physical and chemical characteristics.

The effect of thermal activity was not fully considered in this thesis. Future work could implement thermal models of the cells and position temperature sensors in the battery pack to analyze the changes.

Accurate estimation of SoC could be carried out by accurately modelling the non-linear behaviour of a cell using Extended or Unscented Kalman Filters.

Bibliography

[1] M. Ouyang et al. DOI: https://doi.org/10.1016/j.jpowsour.2015.06.087
[2] Gregory L. Plett, Battery Management Systems: Battery Modeling. Artech House, 2015, Vol. 1.
[3] H. Yang, Shabab Amiruddin, Hyun Joo Bang, Yang-Kook Sun, Jai Prakash, "A review of L-ion cell chemistries and their potential use in hybrid electric vehicles", Center for Electrochemical Science and Engg., Illinois Institute of Technology, pp. 12-38, 2006.
[4] Manh-Kien Tran et al. DOI: https://doi.org/10.3390/a13030062
[5] X. Hu et al. DOI: http://dx.doi.org/10.1109/MIE.2020.2964814.
[6] Feng, X et al. DOI: https://doi.org/10.1016/j.jpowsour.2014.11.017
[7] Lelie, M. et al. DOI: https://doi.org/10.3390/app8040534
[8] Ouyang, D. et al. DOI: https://doi.org/10.1039/C8RA05564E
[9] Fear, C. et al., Elucidating Copper Dissolution Phenomenon in Li-Ion Cells under Overdischarge Extremes. J. Electrochem. Soc. 2018, 165, A1639–A1647.
[10] Doughty, D. et al., General Discussion of Li Ion Battery Safety. Electrochem. Soc. Interface 2012, 21, 37–44.
[11] Wang, H. et al. DOI: https://doi.org/10.1016/j.jpowsour.2015.12.026
[12] Abaza, A. et al., Experimental study of internal and external short circuits of commercial automotive pouch lithium-ion cells. J. Energy Storage 2018, 16, 211–217. DOI: https://doi.org/10.1016/j.est.2018.01.015
[13] Mao, B. et al. DOI: https://doi.org/10.1016/j.ijheatmasstransfer.2018.02.036
[14] Minhwan Seo et al. DOI: http://dx.doi.org/10.12792/icisip2016.038
[15] Lyu, D. et al. DOI: https://doi.org/10.1007/s00707-018-2327-8
[16] Lystianingrum, V et al. DOI: https://doi.org/10.1016/j.jpowsour.2014.09.166
[17] Larsson, F. et al. DOI: https://doi.org/10.1038/s41598-017-09784-z
[18] Galushkin, N.E.; Yazvinskaya, N.N.; Galushkin, D.N. Mechanism of Thermal Runaway in Lithium-Ion Cells. J. Electrochem. Soc. 2018, 165, A1303–A1308
[19] Tran, M.K. et al. DOI: https://doi.org/10.3390/batteries6010001
[20] Liu, Z. et al. DOI: https://doi.org/10.1016/j.conengprac.2016.03.015
[21] Xia, G. et al. J. Power Sources 2017, 367, 90–105 DOI: https://doi.org/10.1016/j.jpowsour.2017.09.046
[22] Yao, L. et al. DOI: https://doi.org/10.1016/j.jpowsour.2015.05.090
[23] X. Feng et al. DOI: https://doi.org/10.1016/j.ensm.2017.05.013
[24] https://www.orbtronic.com/content/samsung-35e-datasheet-inr18650-35e.pdf
[25] LiveLink for Simulink User's Guide

[26] Volck, T. et al. DOI: https://doi.org/10.3390/batteries2020008
[27] Santhanagopalan, S. et al. DOI: https://doi.org/10.1016/j.jpowsour.2009.05.002
[28] Christopher J. Orendorff et al. DOI: https://doi:10.1016/j.jpowsour.2011.03.035
[29] https://www.ntsb.gov/investigations/AccidentReports/Reports/AIR1401.pdf
[30] Xuning Feng et al. DOI: https://doi.org/10.1016/j.ensm.2017.05.013
[31] W. Han, T. Wik, A. Kersten, G. Dong and C. Zou, Next-Generation Battery Management Systems: Dynamic Reconfiguration, in IEEE Industrial Electronics Magazine, vol. 14, no. 4, pp. 20-31, Dec. 2020. DOI: https://doi.org/10.1109/MIE.2020.3002486.
[32] https://www.borregaard.com/markets/batteries/applications/lithium-ion-battery-additives/content-resources/all-you-need-to-know-about-dispersants-for-carbon-in-lithium-ion-batteries/

DEPARTMENT OF ELECTRICAL ENGINEERING
CHALMERS UNIVERSITY OF TECHNOLOGY
GOTHENBURG, SWEDEN
www.chalmers.se

CHALMERS
UNIVERSITY OF TECHNOLOGY